Department of Precision and Microsystems Engineering

The Optimal Sequence for Reset Controllers

Chengwei Cai

Report no : 2019.019
Coach : Dr. Niranjan Saikumar & Ali Ahmadi Dastjerdi
Professor : Dr. Hassan HosseinNia
Specialisation : Mechatronic System Design
Type of report : MSc Thesis
Date : 24.06.2019

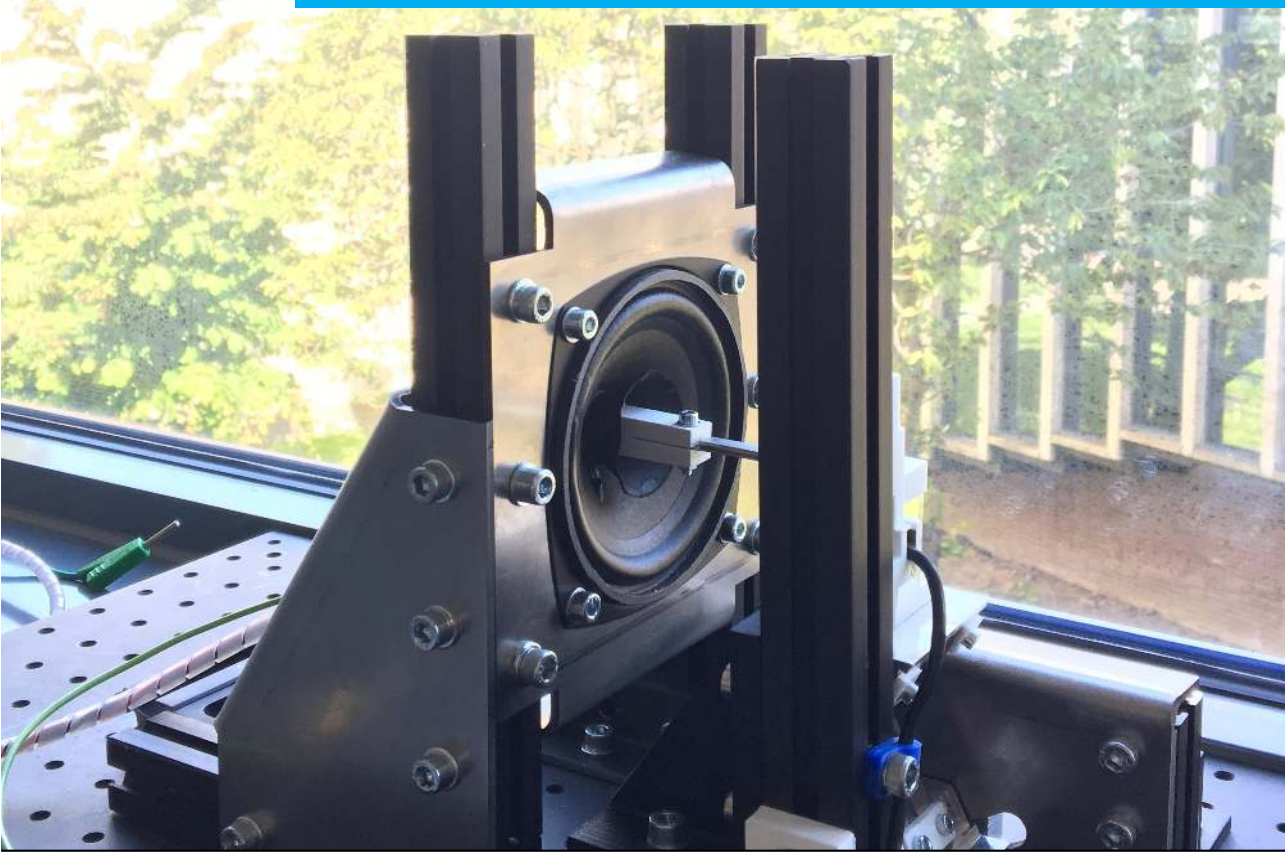

TU Delft Delft University of Technology

Challenge the future

The Optimal Sequence for Reset Controllers

by

Chengwei Cai

For the degree of Master of Science in Mechanical Engineering
at Delft University of Technology,

to be defended publicly on Monday 15th July, 2019 at 10:30 am

Student number:	4707559
Supervisor:	Ali Ahmadi Dastjerdi
	Dr. Niranjan Saikumar
	Dr. Hassan HosseinNia
Thesis committee:	Ir. J. W. Spronck (chairman)
	Dr. Hassan HosseinNia
	Dr. Farbod Alijani

An electronic version of this dissertation is available at
http://repository.tudelft.nl/.

TU Delft Delft University of Technology

Contents

1 Introduction **1**

2 Literature Review **3**

3 Objective **11**
3.1 Problem Definition . . . 11
3.2 Research Approach . . . 11
3.3 Thesis Outline . . . 12

4 The Optimal Sequence for Reset Controllers **13**

5 Conclusion **23**

A HOSIDOFs of Different Sequences **25**
A.1 The optimal sequence in open loop . . . 25
A.2 Illustrative example . . . 25

B HOSIDOFs with Shaping Filter **29**

C Shaping Filter for Noise Attenuation **33**

D Trajectory Tracking Performance **37**

E Shaping Filter for Less Phase Lag **41**

F System Overview **43**
F.1 Setup . . . 43
F.2 Identification . . . 44

G Matlab Code and Simulink Model **47**
G.1 HOSIDOFs.m . . . 47
G.2 Identification.m . . . 48
G.3 Sensitivityfunction.m . . . 49
G.4 hosidfcalc.m . . . 51
G.5 Simulink model . . . 52

Bibliography **55**

Preface

This report is the final part of my master program in High-Tech Engineering (HTE) track at TU Delft. Now looking back over the past two years, every bit of life and study in delft has left a precious imprint on my memory. During this time, countless people have helped me and made me a better person. This work could never have been realized without the help of the following people, who I want to thank in particular:

Ali Ahmadi Dastjerdi: As my daily supervisor, thank you for your professional and patient guidance during each meeting. Whenever I encountered difficulties and felt depression, it was your positive encouragement that gave me the power to move on.

Niranjan Saikumar: Thank you for your powerful support of programming the Labview code and conducting the experiment. It was your priceless advice and concern that kept my work always on track.

Hassan HosseinNia: Thank you for providing me such an exciting project in which I can apply theoretical knowledge in practise. Your encouragement made an introverted student learn to express his own opinion bravely and benefit a lot from this process.

Friends at HTE department: Especially from Jo and Hassan's group, for all suggestions and inspirations from each Monday meeting, which helped a lot to improve my work.

My family: The warm companionship of my girlfriend when I walked through all of this. My parents who gave me unlimited trust and support when I doubt myself.

Chengwei Cai
Delft, June 2019

1

Introduction

Today, high-tech development is faster than most people's imagination. A typical representative is the most sophisticated mechanical system presently available which is the stages of wafer scanners used in the semiconductor industry [1]. Figure 1.1 shows the development of the lithography machines of ASML. Within just 20 years, the resolution has been enhanced from $1\mu m$ to 20 nm. This transformation, which is like transformation from toddling to dancing on the tip of knifes, allows the Moore's law [2] to continue.

Figure 1.1: Overview of lithography machines from ASML [3]

In order to achieve this kind of extraordinary task, precision positioning technology plays an important role inside. To ensure the high quality of productions, nano-precision controllers with high bandwidth and stability are required in these applications.

1

The PID controller is by far the most dominating form of feedback in use today [4]. It is versatile and widely used in general cases of motion control applications because of simple structure and tuning rule. However, when higher bandwidth and accuracy are required while maintaining stability margin in precision systems, it becomes harder to fulfill the requirements only using conventional PID controllers. Because of their linear nature, fundamental limitations of linearity such as water-bed effect and bode gain phase relationship [5] restrict PID especially in high precision instruments. Although many non-linear control theories have been developed to overcome these limitations, most of them have complex structure and their tuning methods are very complicated. Among them, reset controllers have attracted a lot of attention from academic institution and industry due to their simple structures [6], [7], [8], [9], [10].

Reset control is a novel kind of nonlinear control strategies which has been developed since 1958. A traditional reset element resets its own state to zero every time the input signal crosses the zero point. Clegg first proposed the concept of reset by applying reset control strategy on a linear integrator in [11]. From Describing Function (DF) analysis in [12], Clegg integrator has a similar gain behavior with the basic linear integrator while it reduces the phase lag from -90° to -38°. After the inspiration of Clegg integrator, First Order Reset Element(FORE) and Second Order Reset Element(SORE) were developped [13][14] which makes it possible to apply reset controllers on more complex systems and get benefit from it.

Unlike linear controllers, the sequence of different parts in non-linear controllers has effects on performance of the systems because of high order harmonics. While the reset control has been used in a wide range of applications, the influence of different sequences is not found in literature to the best of authors' knowledge.

This thesis aims to find the best sequence of controllers when there is a reset element among them. Although DF is widely used to analyze and tune reset controllers in frequency domain, this method does not consider high order harmonics which affect the performance of the systems. In order to investigate the influence of high order harmonics in general non-linear systems, Nuij proposed the concept of high order sinusoidal input describing functions (HOSIDFs) in [15]. Based on that theory, Kars developed HOSIDOFs for reset elements in [16]. In order to find the optimal sequence of controllers when there is a reset element, HOSIDOFs tool is used in this study.

2

Literature Review

This chapter presents the literature review part of the thesis in paper format. Firstly, the fundamental knowledge of reset control is introduced. Secondly, high order harmonics within reset elements and the problems they caused are investigated. Finally, different strategies of applying reset elements in literature are shown and discussed.

Literature review: Reset control and influence of high order harmonics

Chengwei Cai, A.A. Dastjerdi, and S.Hassan HosseinNia

***Abstract*—Linear PID controller is one of the most widely used controllers in industry owning to simplicity and ease of tuning. However, new control requirements due to the development of technology is now pushing PID and other linear controllers to their limitation. To overcome the limitations such as Bode gain-phase relationship and water bed effect, many non-linear controllers have been developed. Among them, reset control elements have attracted a lot of attention because of their simplicity and flexibility. However, reset controllers also introduce high order harmonics into the system which can induce limit cycle and deteriorate the performance. This paper mainly reviews different strategies of applying reset elements in literature and the influence of high order harmonics caused by non-linearity.**

I. Introduction

The PID controller is by far the most dominating form of feedback in use today [1]. PID is abbreviation for three different components: Proportional(P) element, Integral(I) element and Derivative(D) element. It is versatile and widely used in general cases of motion control applications because of simple structure and tuning rule. The Proportional element is used to set the desired bandwidth we would like to reach; Integral element creates high gain at low frequency and Derivative element can provide phase lead around the crossover frequency.

However, when higher bandwidth and accuracy are required while maintaining stability margin in precision systems, it becomes harder to fulfill the requirement only use conventional PID controllers. Because of their linear nature, fundamental limitations of linearity restrict PID and other linear controllers' applications especially in high precision instruments.

One of the limitations of linear controller is the phase-gain relationship in Bode plot. For a stable Minimum Phase System (MPS), there exists an unique relation between the gain and phase of a frequency response function [2]:

$$\angle G(j\omega_0) = 90^\circ N(j\omega_0)$$

where N is the slope of gain in Bode plot.

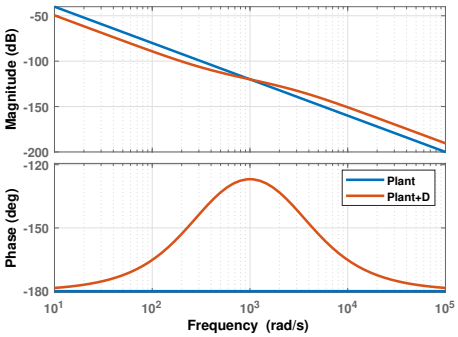

Figure 1: Bode Gain-Phase relationship

As shown in Fig.1, the blue line represents a single mass system with -2 slope and -180° phase. In order to control this marginal stable system, we add a tamed derivative element to provide phase lead at the required bandwidth. The whole system's transfer function then can be illustrated by the red line. Although the derivative element creates enough phase margin to ensure stability, because of the slope change in the magnitude plot, lower gain in low frequencies and higher gain in high frequencies are inevitable. According to the loop shaping, the decreasing slope deteriorates the tracking performance and noise attenuation. Therefore, we always need to trade off between system's performance and stability when using linear controllers .

Another basic limitation of linear controller is called water-bed effect, which can be indicated by the Bode Sensitivity Integral [3]:

$$\int_0^\infty \ln|S(\omega)|d\omega$$

The above integral is always 0 for a stable feedback system, which means it is impossible to have good disturbance rejection for all frequencies.

These limitations and trade off are elaborated in [2] and [3]. Although many other advanced control theories have been developed, most of them have complex structure and their tuning methods are very complicated. Among these non-linear controllers, reset controllers have attracted a lot of attention from academic institution and industry due to their simple structures [4], [5], [6], [7].

Reset control is a novel kind of nonlinear control strategy which has been developed since 1958. For a traditional

reset element, the state is reset to zero every time the input signal crosses zero. Clegg first introduced this concept in 1958 by applying reset action on a linear integrator. The time domain responses of Clegg integrator and the linear integrator are compared in Fig.2 with a sinusoidal input signal. It is clear that each instant the input signal cross 0, reset action will be triggered and reset the output of Clegg integrator to 0.

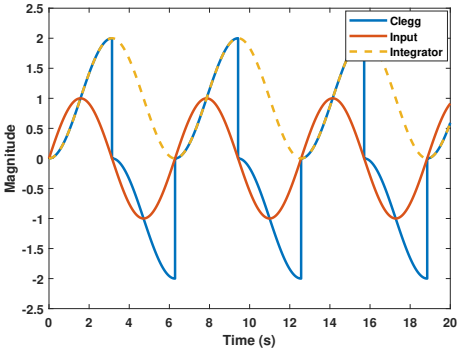

Figure 2: Time domain response of Clegg integrator and linear integrator

The frequency domain response of Clegg integrator is achieved by describing function (DF) analysis [8] and compared with linear integrator in Fig.3.

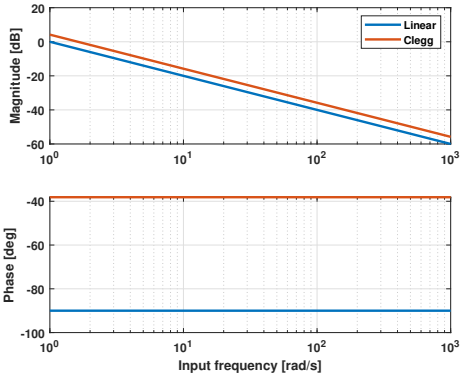

Figure 3: Bode plot of Clegg integrator and linear integrator

It showns that Clegg integrator has a similar gain behavior with the basic linear integrator, while it reduces the phase lag from 90° to 38°. This property is profitable in terms of improving the system's performance without sacrificing stability. After the inspiration of reset integrator, many researchers realized the potential of reset control strategy and have conducted further investigation. In [9] and [10], Horowitz et al. and Hazelgar et. al. extended the investigation to First Order Reset Element(FORE) and Second Order Reset Element(SORE), which make it possible to apply reset control technology on more complex systems and get benefit from it. Until now, the reset control technology has been used in a wide range of applications, some relative work can be found in hard drive disk systems [11], [12], precision stages [13], [14], servo systems [15], [16], etc.

Although DF is widely used to analyze and tune reset controllers in frequency domain, this method does not consider high order harmonics. Especially in precision systems, these high order harmonics' effect are inevitable and can lead to unwanted dynamics which deteriorate system's performance seriously.

In order to investigate the influence of high order harmonics in non-linear systems, Nuji proposed the theory of High Order Sinusoidal Input Describing Functions (HOSIDOFs) in [17]. Based on this, Heinen developed HOSIDOFs for reset elements in [18].

This paper provides an overview of reset control theory and problems caused by high order harmonics. Tools to analyze reset elements and existing strategies to deal with the problems caused by high order harmonics are also illustrated. The basic knowledge of reset control and tools to analyze it are provided in section II. Problems caused by high order harmonics are stated in section III. Existing strategies to deal with these problems are presented in section IV followed by the conclusion.

II. Preliminary

A. Reset control

A general reset controller is defined by the following state space equations according to [19]:

$$\Sigma_R = \begin{cases} \dot{x}_r(t) = A_r x_r(t) + B_r e(t) & \text{if } e(t) \neq 0 \\ x_r(t^+) = A_\rho x_r(t) & \text{if } e(t) = 0 \\ u(t) = C_r x_r(t) + D_r e(t) & \end{cases} \quad (1)$$

Where A_r, B_r, C_r, D_r are state space matrices of the corresponding base linear system. A_ρ is reset matrix determining the state after reset values [20], $e(t)$ is error signal between reference and output and $u(t)$ is the whole controller's output.

To simplify the design of the reset controller, reset matrix A_ρ is often defined as diagonal form:

$$A_\rho = \gamma I_{n\times n}$$

where n is the order of the reset controller and γ is reset value. Reset action is triggered according to reset law. In traditional reset elements, $e(t) = 0$ is considered as the reset law.

1) Clegg Integrator (CI): Clegg or reset integrator is a kind of nonlinear integrator first proposed by J. C. Clegg in [21]. By applying a reset action on a linear integrator, Clegg integrator has a similar gain behavior with the linear one in frequency domain while the phase lag is reduced

from 90° to 38.1°. The state space matrices and reset matrix of Clegg integrator in (1) are:

$$A_r = 0;\ B_r = 1;\ C_r = 1;\ D_r = 0;\ A_\rho = 0$$

2) First Order Reset Element (FORE): Horowitz and P. Rosenbaum applied reset action on a first order low-pass filter (LPF) [9]. This extended CI to a First Order Reset Element (FORE). The state space matrices and reset matrix of FORE in (1) are:

$$A_r = -\omega_r;\ B_r = \omega_r;\ C_r = 1;\ D_r = 0;\ A_\rho = 0$$

Where ω_r is the basic low-pass filter's corner frequency.

Fig.4 shows the bode plot of a FORE and the basic LPF. It is clear that phase lead is achieved after ω_r comparing with the linear LPF.

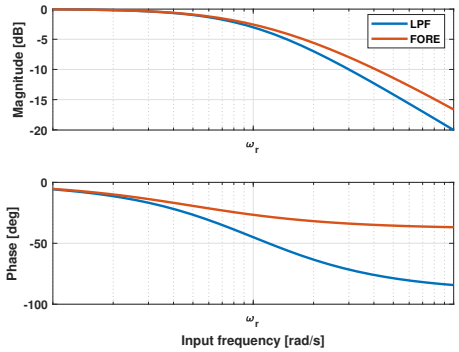

Figure 4: Bode plot of FORE and LPF

3) Second Order Reset Element(SORE): Hazeleger applied reset action on a second order LPF in [10] to generate Second Order Reset Element(SORE). The state space matrices of SORE in (1) are:

$$A_r = \begin{bmatrix} 0 & 1 \\ -\omega_r^2 & -2\beta\omega_r \end{bmatrix};\ B_r = \begin{bmatrix} 0 \\ \omega_r^2 \end{bmatrix};$$

$$C_r = \begin{bmatrix} 1 & 0 \end{bmatrix};\ D_r = [0]$$

Where ω_r is the corner frequency of the basic second order LPF, β is damping ratio. More flexibility can be achieved by the additional parameter. Fig.5 shows the bode plot of SORE with different damping ratio when we set reset value γ=0.

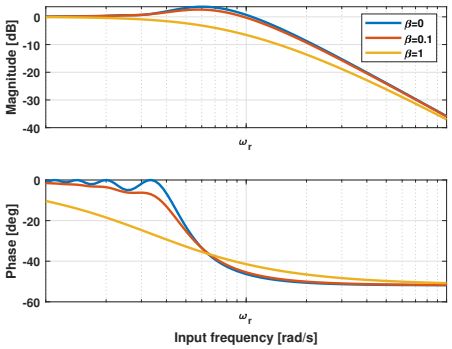

Figure 5: Bode plot of SORE for different β_r

B. Describing function

In order to design and tune reset controllers for specific systems, the investigation of frequency-domain properties for reset controllers is significant.

In [8], the sinusoidal input describing function (DF) of a general reset system has been developed. The sinusoidal input describing function theory assumed there is a quasi-linear amplitude-dependent relation between sinusoidal excitation and sinusoidal response [17]. Derived from (1), the DF of a general reset element for a sinusoidal input is achieved as:

$$G(j\omega) = C_r^T \left(j\omega I - A_r\right)^{-1} \left(I + j\Theta_\rho(\omega)\right) B_r + D_r \qquad (2)$$

where

$$\Theta_\rho = \frac{2}{\pi}\left(I + e^{\frac{\pi A_r}{\omega}}\right)\left(\frac{I - A_\rho}{I + A_\rho e^{\frac{\pi A_r}{\omega}}}\right)\left(\left(\frac{A_r}{\omega}\right)^2 + I\right)^{-1}$$

C. HOSIDFs

In order to investigate the influence of high order harmonics in general non-linear systems, Nuij proposed the concept of high order sinusoidal input describing functions (HOSIDFs) in [17].

The basic skeleton of high order sinusoidal describing functions (HOSIDFs)when a linear part is in series with a nonlinear part is shown in Fig. 6.

In this block representation, the non-linear part is divided into two different parts: virtual harmonic generator part and describing function part. For the sake of explanation, we define the describing function of n order harmonic as $G(nj\omega)$. Different order of harmonics are generated by virtual harmonic generator and contribute to final output by multiplying corresponding order describing function. These describing functions can be calculated by method based on Fourier series. For reset controllers, HOSIDOFs depends not only the reset matrix and state space matrices of the system, but also the reset rules. Based on this

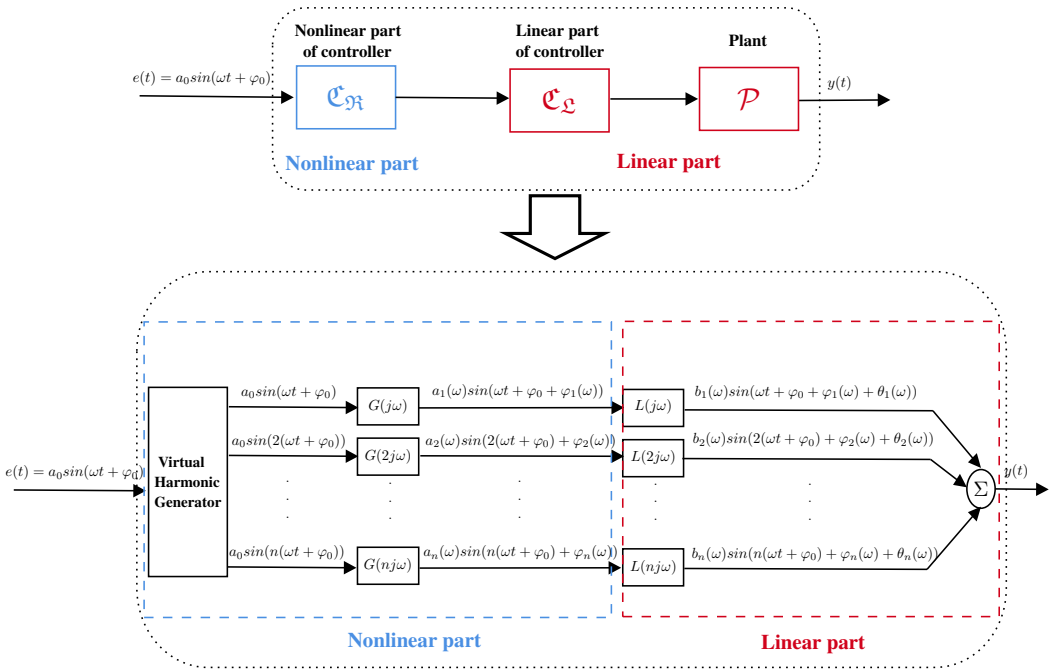

Figure 6: HOSIDOFs Representation

theory, Heinen developed the HOSIDOFs of a general reset element in [18] as: $G(nj\omega) =$

$$\begin{cases} C_r(j\omega I - A_r)^{-1}(I + j\Theta_\rho(\omega))B_r + D_r & \text{for } n = 1 \\ C_r(j\omega n I - A_r)^{-1} j\Theta_\rho(\omega) B_r & \text{for } odd\ n \geq 2 \\ 0 & \text{for } even\ n \geq 2 \end{cases} \tag{3}$$

III. Challenges toward reset controllers

A. Reliability of the first order describing function

Although DF is widely used to analyze and tune reset controllers in frequency domain, this method does not consider high order harmonics which affect the performance of the system. With (3), reset elements' HOSIDFs can be calculated conveniently. Consider a First Order Reset Element(F0RE) with state space matrices and reset matrix:

$$A_r = -10;\ B_r = 10;\ C_r = 1;\ D_r = 0;\ A_\rho = 0$$

The HOSIDFs are illustrated in Fig. 7.

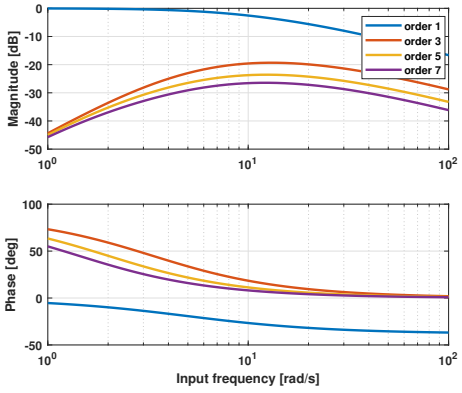

Figure 7: HOSIDFs of FORE

It is clear that apart from the first order describing function which is represented by the blue line, the FORE also contains high order describing functions. Because there is no reliable approach to combine different order describing function together, we can only tune our system according to the first order describing function.

Difference between the first order describing function and the real nonlinear system makes it impossible to tune the real system precisely, therefore deteriorate system's

performance. For the FORE in Fig. 7, the worst situation appears at around the corner frequency ($10Hz$), where the magnitudes of high order harmonics reach their maximum value and are closed to the magnitude of the first order one.

Deterioration of performance because of high order harmonics has been observed by experiments in [22], [23] and [24].

B. Limit cycle

Limit cycle is a common problem caused by high order harmonics in reset elements. It occurs because the controller's output after reset action is not equal to the steady state value. Consider a linear PI controller $\mathfrak{C}_{\mathfrak{L}}$ and a corresponding reset PI controller $\mathfrak{C}_{\mathfrak{R}}$ as given below:

$$\mathfrak{C}_{\mathfrak{L}} = \begin{cases} \dot{x}_r(t) = 0 \times x_r(t) + 1 \times e(t) \\ u(t) = 10 \times x_r(t) + 1 \times e(t) \end{cases} \tag{4}$$

$$\mathfrak{C}_{\mathfrak{R}} = \begin{cases} \dot{x}_r(t) = 0 \times x_r(t) + 1 \times e(t) & \text{if } e(t) \neq 0 \\ x_r(t^+) = 0 & \text{if } e(t) = 0 \\ u(t) = 10 \times x_r(t) + 1 \times e(t) \end{cases} \tag{5}$$

Apply them separately in a close loop for a plant with transfer function: $\frac{1}{s+0.5}$.

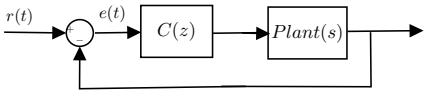

Figure 8: Feedback loop

The step responses of this two controllers are shown in Fig. 9:

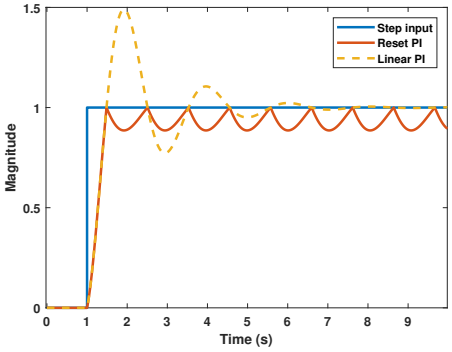

Figure 9: Step response of linear PI and reset PI

Comparing with the linear PI controller, the reset PI controller reduces the overshoot of step response. In addition, the settling time is much shorter than the linear one (if we define the settling band as $\pm 15\%$). However, instead of stabilizing at the reference value, a periodical oscillation occurs in the reset PI case after settling time. This kind of persistent oscillation is called limit cycle. Obviously, limit cycle can lead to steady state error and deteriorate whole system's performance, which is undesired in precision applications.

IV. Existing strategies of reset control

The existence of high order harmonics is inevitable in reset controllers. To deal with the problems caused by high order harmonics such as limit cycle, several strategies have been developed in literature to soft the degree of nonlinearity.

A. Partial reset

As we mentioned in section II, γ within A_ρ is the reset value determining the state after reset action. In traditional reset elements, γ is set to 0, which means complete reset. Partial reset can be realized by tuning γ between 0 and 1.

Fig. 10 shows the step response of the same reset PI controller when we change γ to different values. Although the limit cycle still occurs, the amplitude of it decreases when we increase γ.

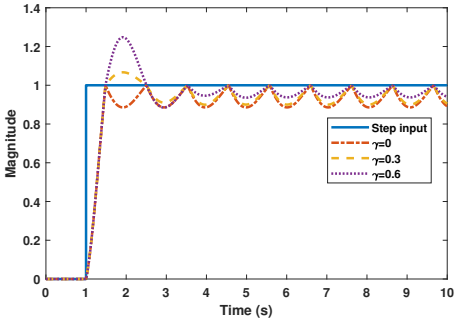

Figure 10: Step response for different γ

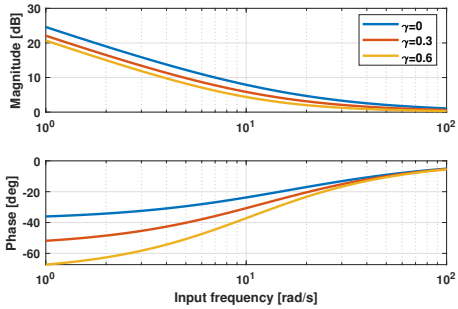

Figure 11: First order describing function for different γ

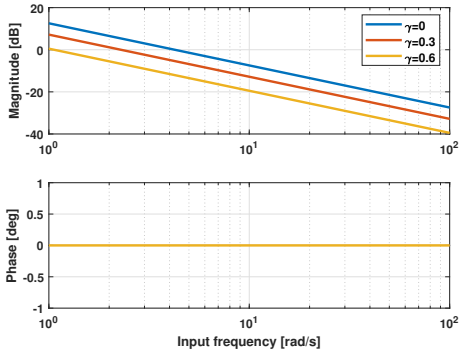

Figure 12: Third order describing function for different γ

In Fig. 11 and Fig. 12, the first and third order describing functions of the reset PI for different γ are plotted.

When γ increases, the phase lead benefit decreases in Fig. 11. However, in Fig. 12, magnitude of high order harmonics also decreases with rising γ, which means system can suffer less from high order harmonics. By tuning γ between 0 and 1, partial reset makes it possible to find an optimized point between phase lead benefit and influence of high order harmonics.

B. PI+CI

Another strategy to tune system's degree of non-linearity is PI+CI configuration. The structure of PI+CI is shown in Fig. 13:

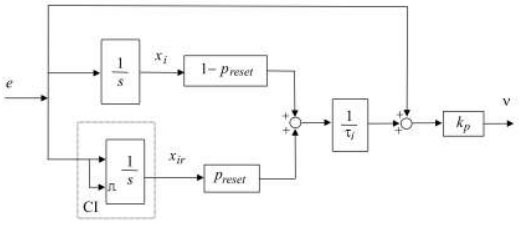

Figure 13: block diagram of PI+CI [25]

The main idea is adding an additional Clegg integrator to a traditional PI controller and connecting it in parallel to the linear one. The degree of non-linearity can be tuned by varying constant gain P_{reset}. This controller then can be represented by:

$$PI + CI = k_p(1 + \frac{1}{\tau_i}(\frac{1 - P_{reset}}{s} + \frac{P_{reset}}{\not{s}})) \qquad (6)$$

Again use the same basic linear PI controller and set $P_{reset} = 0.8$. The step response of PI+CI controller, Reset PI controller and linear PI controller are compared in Fig. 14:

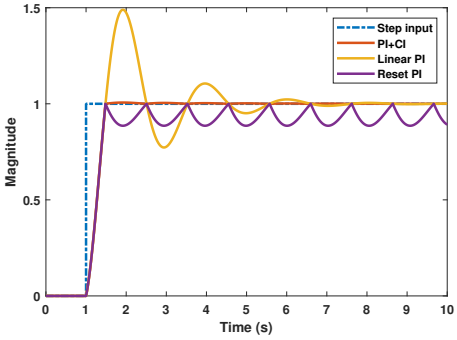

Figure 14: Step response of PI+CI, Linear PI and Reset PI

It is clear that in $PI + CI$ case, limit cycle disappears because the linear PI part helps remove the steady state error. Also, the response has much less overshoot and settling time comparing with linear PI controller, which is the benefit from reset part. An optimal and systematic tuning rule for PI+CI controller has been summarized in [26]. More relative application can be found in [27], [28] and [29].

C. Reset band

Previous reset elements all have the same reset rule: $e(t) = 0$, which means reset action will be triggered each time error signal crosses zero. Reset band strategy is realized by triggering the reset action each time error signal enters a specific band. A general reset band element can be described by the following equations:

$$\Sigma_R = \begin{cases} \dot{x}_r(t) = A_r x_r(t) + B_r e(t) & \text{if } e(t), \dot{e(t)} \notin B_\delta \\ x_r(t^+) = A_\rho x_r(t) & \text{if } e(t), \dot{e(t)} \in B_\delta \\ u(t) = C_r x_r(t) + D_r e(t) \end{cases} \qquad (7)$$

where $B_\delta = (x, y) \in R^2 | (x = -\delta \wedge y > 0) \vee (x = \delta \wedge y < 0)$.

Band reset strategy is especially suitable for systems with time delay, because it can provide even more phase lead than traditional reset element which resets according to zero crossing. It also has been proven that reset band can be used to remove limit cycle in some cases. However, the performance of band reset strategy is decided by reset band parameter δ, which is hard to design when system uncertainty occurs.

V. Conclusions

Reset controllers have attracted a lot of attention from academic institution and industry due to their simple structures and ability to overcome the limitations of linear controllers.

Most of reset control design in literature relays on Describing function(DF). Although DF is a useful tool

to investigate reset system's performance in frequency domain, it does not consider high order harmonics. Especially in precision positioning applications, the influence of high order harmonics can not be omitted and may even lose the benefits of reset controllers.

To deal with the problems caused by high order harmonics such as limit cycles and unwanted dynamic, several reset strategies have been proposed in literature, such as Partial reset, PI+CI and Reset band. Partial reset can soft the influence of high order harmonics, but it also sacrifices the phase lead benefit at the same time. Also, it is not able to remove the limit cycle effectively. PI+CI strategy appears to solve the limit cycle problem successfully. But it is still a trade off between linearity and non-linearity, which wastes some potential of reset elements. For Reset band, although it performs well in some ideal cases, it is not robust enough for systems with uncertainty in reality.

Above all, the influence of high order harmonics has become an important limitation for the development of reset control. Although HOSIDFs theory has been developed and is a powerful tool to visualize the influence of high order harmonics, research about HOSIDFs on design of reset controllers is still lack within literature.

References

[1] K. J. Åström and T. Hägglund, "The future of PID control," *Control engineering practice*, vol. 9, no. 11, pp. 1163–1175, 2001.

[2] S. Skogestad and I. Postlethwaite, *Multivariable feedback control: analysis and design*. Wiley New York, 2007, vol. 2.

[3] R. M. Schmidt, G. Schitter, and A. Rankers, *The Design of High Performance Mechatronics-: High-Tech Functionality by Multidisciplinary System Integration*. Ios Press, 2014.

[4] L. Chen, N. Saikumar, S. Baldi, and S. H. HosseinNia, "Beyond the waterbed effect: Development of fractional order crone control with non-linear reset," in *2018 Annual American Control Conference (ACC)*. IEEE, 2018, pp. 545–552.

[5] M. Zarghami and S. HassanHosseinNia, "Fractional order set point regulator using reset control: Application to egr systems," in *Proceedings of the 2017 The 5th International Conference on Control, Mechatronics and Automation*. ACM, 2017, pp. 35–41.

[6] S. H. HosseinNia, I. Tejado, and B. M. Vinagre, "Basic properties and stability of fractional-order reset control systems," in *2013 European Control Conference (ECC)*. IEEE, 2013, pp. 1687–1692.

[7] ——, "Fractional-order reset control: Application to a servomotor," *Mechatronics*, vol. 23, no. 7, pp. 781–788, 2013.

[8] Y. Guo, Y. Wang, and L. Xie, "Frequency-domain properties of reset systems with application in hard-disk-drive systems," *IEEE Transactions on Control Systems Technology*, vol. 17, no. 6, pp. 1446–1453, 2009.

[9] I. Horowitz and P. Rosenbaum, "Non-linear design for cost of feedback reduction in systems with large parameter uncertainty," *International Journal of Control*, vol. 21, no. 6, pp. 977–1001, 1975.

[10] L. Hazeleger, M. Heertjes, and H. Nijmeijer, "Second-order reset elements for stage control design," in *American Control Conference (ACC), 2016*. IEEE, 2016, pp. 2643–2648.

[11] Y. Li, G. Guo, and Y. Wang, "Reset control for midfrequency narrowband disturbance rejection with an application in hard disk drives," *IEEE Transactions on Control Systems Technology*, vol. 19, no. 6, pp. 1339–1348, 2011.

[12] H. Li, C. Du, and Y. Wang, "Discrete-time h 2 optimal reset control with application to hdd track-following," in *2009 Chinese Control and Decision Conference*. IEEE, 2009, pp. 3613–3617.

[13] ——, "Optimal reset control for a dual-stage actuator system in hdds," *IEEE/ASME Transactions on Mechatronics*, vol. 16, no. 3, pp. 480–488, 2011.

[14] J. Zheng, Y. Guo, M. Fu, Y. Wang, and L. Xie, "Improved reset control design for a pzt positioning stage," in *2007 IEEE International Conference on Control Applications*. IEEE, 2007, pp. 1272–1277.

[15] Y. Li, G. Guo, and Y. Wang, "Phase lead reset control design with an application to hdd servo systems," in *2006 9th International Conference on Control, Automation, Robotics and Vision*. IEEE, 2006, pp. 1–6.

[16] D. Wu, G. Guo, and Y. Wang, "Reset integral-derivative control for hdd servo systems," *IEEE Transactions on Control Systems Technology*, vol. 15, no. 1, pp. 161–167, 2007.

[17] P. Nuij, O. Bosgra, and M. Steinbuch, "Higher-order sinusoidal input describing functions for the analysis of non-linear systems with harmonic responses," *Mechanical Systems and Signal Processing*, vol. 20, no. 8, pp. 1883–1904, 2006.

[18] K. Heinen, "Frequency analysis of reset systems containing a clegg integrator: An introduction to higher order sinusoidal input describing functions," 2018.

[19] A. Baños and A. Barreiro, *Reset control systems*. Springer Science & Business Media, 2011.

[20] N. Saikumar, R. K. Sinha, and S. H. HosseinNia, "'constant in gain lead in phase'element-application in precision motion control," *arXiv preprint arXiv:1805.12406*, 2018.

[21] J. Clegg, "A nonlinear integrator for servomechanisms," *Transactions of the American Institute of Electrical Engineers, Part II: Applications and Industry*, vol. 77, no. 1, pp. 41–42, 1958.

[22] N. Saikumar, R. Sinha, and S. H. Hoseinnia, "'constant in gain lead in phase'element-application in precision motion control," *IEEE/ASME Transactions on Mechatronics*, 2019.

[23] Y. Salman, "Tuning a novel reset element through describing function and hosidf analysis," october 31, 2018.

[24] E. Akyüz, "Reset control for vibration isolation," october 31, 2018.

[25] A. Barreiro, A. Baños, S. Dormido, and J. A. González-Prieto, "Reset control systems with reset band: Well-posedness, limit cycles and stability analysis," *Systems & Control Letters*, vol. 63, pp. 1–11, 2014.

[26] A. Baños and A. Vidal, "Definition and tuning of a pi+ ci reset controller," in *Control Conference (ECC), 2007 European*. IEEE, 2007, pp. 4792–4798.

[27] A. Banos and A. Vidal, "Design of pi+ ci reset compensators for second order plants," in *Industrial Electronics, 2007. ISIE 2007. IEEE International Symposium on*. IEEE, 2007, pp. 118–123.

[28] A. F. Villaverde, A. B. Blas, J. Carrasco, and A. B. Torrico, "Reset control for passive bilateral teleoperation," *IEEE Transactions on Industrial Electronics*, vol. 58, no. 7, pp. 3037–3045, 2011.

[29] A. Vidal and A. Baños, "Reset compensation for temperature control: Experimental application on heat exchangers," *Chemical Engineering Journal*, vol. 159, no. 1-3, pp. 170–181, 2010.

3

Objective

3.1. Problem Definition

The literature review part shows the state of art for reset control strategy. Although reset elements have attracted a lot of attention because of their simplicity and ability to overcome the limitation of linear controllers, high order harmonics are introduced because of non-linearity. High order harmonics deteriorate the performance of reset controllers, so it is necessary to reduce them as much as possible. Using HOSIDOFs tool, it is found that the sequence of different parts of a reset controller has effect on the magnitude of high order harmonics. Based on this, the objective of this thesis is set as:

Find the optimal sequence for reset controllers which has the smallest magnitude of high order harmonics and check if this sequence has the best performance in closed loop.

3.2. Research Approach

The research is conducted by the following approach:

- Use HOSIDOFs tool to investigate the magnitude of high order harmonics for a general reset controller with different sequence of controller parts.
- Find the optimal general sequence in open loop which has the smallest magnitude of high order harmonics.
- Check the closed-loop performance of different sequences in Matlab simulation.
- Validate the superiority of the optimal sequence in closed-loop configuration at a Lorentz-actuated precision positioning stage.

3.3. Thesis Outline

The thesis is structured as follows.

Chapter 1 provides a brief introduction of motion control especially in high tech industry applications. In Chapter 2, the state of art for reset control strategy within literature is elaborated. This chapter provides the objective of the thesis work and the research approach to achieve the objective. The core part of this thesis, an investigation of the optimal sequence for reset controllers is presented in Chapter 4 as scientific paper format. Chapter 5 shows the conclusion and recommendation for future research. More details during the thesis work are attached in the Appendices.

4

The Optimal Sequence for Reset Controllers

This chapter is presented in a scientific paper format. Although reset controllers have been widely used to overcome the limitation of linear controllers in literature, performances of the system can be different depending on the relative sequence of controller parts. In this paper, the optimal sequence has been derived utilizing(HOSIDFs). By arranging controller parts according to this strategy, the superiority in the sense of precision and control output has been validated in the closed-loop configuration at a Lorentz-actuated precision positioning stage.

The optimal sequence for reset controllers

Chengwei Cai, A.A. Dastjerdi, Niranjan Saikumar, S. Hassan HosseinNia

***Abstract*—Today, high-tech precision industry is faced with new control requirements due to the development of technology. Some researchers believe that using non-linear controllers can satisfy these requirements. Among non-linear controllers, reset elements have attracted a lot of attention because of their simplicity. Although reset controllers have been widely used to overcome the limitation of linear controllers in literature, performances of the system can be different depending on the relative sequence of controller parts. In this paper, the optimal sequence has been derived from the investigation of high order sinusoidal input describing functions(HOSIDFs). By arranging controller parts according to this strategy, the superiority in the sense of precision and control output has been validated in closed-loop configuration at a Lorentz-actuated precision positioning stage. In conclusion, using this sequence for reset controllers improves the performances of the system from precision perspective.**

***Keywords*—Reset controllers, Optimal sequence, HOSIDFs, Precision positioning**

I. Introduction

Precision positioning is an important topic in high-tech industry such as lithography machines. In these applications, nano-precision controllers with high bandwidth and stability are required to ensure the high quality of productions. PID controllers, which are one of the most used controllers in industry owning to their simplicity and ease of tuning, can not fulfill these control requirements due to their linear nature. Water-bed effect confines performances of linear controllers so that it is impossible to achieve high bandwidth, stability and precision simultaneously [1], [2]. Many advanced nonlinear controllers have been developed recent years to overcome the limitation of linearity. However, most of them have complex structure and their tuning methods are very complicated. Among these non-linear controllers, reset controllers have attracted a lot of attention from academic institutions and industry due to their simple structures [3], [4], [5], [6], [7].

Reset control is a novel kind of nonlinear control strategy which has been developed since 1958. A traditional reset element resets its own state to zero when the input signal crosses zero. Clegg first proposed the concept of reset by applying reset control strategy on a linear integrator in [8]. From Describing Function (DF) analysis in [9], Clegg integrator has a similar gain behavior with the basic linear integrator while it reduces the phase lag from -90° to -38°. This property is profitable in terms of improving the system's performance without sacrificing stability. In [10] and [11], Horowitz et al. and Hazelgar et. al. extended the investigation to First Order Reset Element (FORE) and Second Order Reset Element (SORE) which make it possible to apply reset control on more complex systems and get benefit from it. Also, several strategies have been developed to tune the degree of non-linearity of reset elements such as partial reset, PI+CI, reset band and fixed time reset [12], [13], [14], [15]. The reset control has been used in a wide range of applications [16], [17], [18], [19], [20].

Although DF is widely used to analyze and tune reset controllers in frequency domain, this method does not consider high order harmonics which affect the performance of the system. In order to investigate the influence of high order harmonics in general non-linear systems, Nuij proposed the concept of high order sinusoidal input describing functions (HOSIDFs) in [21]. The representation of HOSIDOFs when a linear part is in series with a nonlinear part is shown in Fig. 1. Based on that theory, Kars developed HOSIDOFs for reset elements in [22].

High order harmonics deteriorate the performance of reset controllers, so it is necessary to reduce them as much as possible. Using HOSIDOFs tool, it is found that the sequence of different parts of a reset controller has effect on the magnitude of high order harmonics. This paper aims to reduce the side effects of high order harmonics by changing the relative sequence of controller parts. The best arrangement will be selected to have best precision and reduce control sensitivity output. Then, this arrangement's performance is examined on simulation and a real precision setup.

In the remainder of this paper, in section II, preliminary knowledge about reset controllers and mathematical tools to investigate frequency domain of nonlinear systems are presented. Theoretical investigation about different sequences of controller parts is presented in section III. In section IV, the simulation result for closed-loop configuration is presented. The experimental results and conclusion are described in sections V and VI, separately.

II. Preliminary

A. Reset Control

A general reset controller is defined by the following state-space equations according to [23]:

$$\Sigma_R = \begin{cases} \dot{x}_r(t) = A_r x_r(t) + B_r e(t) & \text{if } e(t) \neq 0 \\ x_r(t^+) = A_\rho x_r(t) & \text{if } e(t) = 0 \\ u(t) = C_r x_r(t) + D_r e(t) & \end{cases} \quad (1)$$

where A_r, B_r, C_r and D_r are state-space matrices of the corresponding base linear system. A_ρ is reset matrix determining the state values after reset action, $e(t)$ is error input and $u(t)$ is the whole controller's output.

To simplify the design of the reset controller, reset matrix A_ρ is often defined as diagonal form:

$$A_\rho = \gamma I_{n\times n}$$

where n is the order of the reset controller and γ is reset value. Reset action is triggered according to reset law. In this paper, $e(t) = 0$ is considered as reset law.

Describing function of a general reset element for a sinusoidal input is achieved in [9] as:

$$G(j\omega) = C_r^T(j\omega I - A_r)^{-1}(I + j\Theta_\rho(\omega))B_r + D_r \quad (2)$$

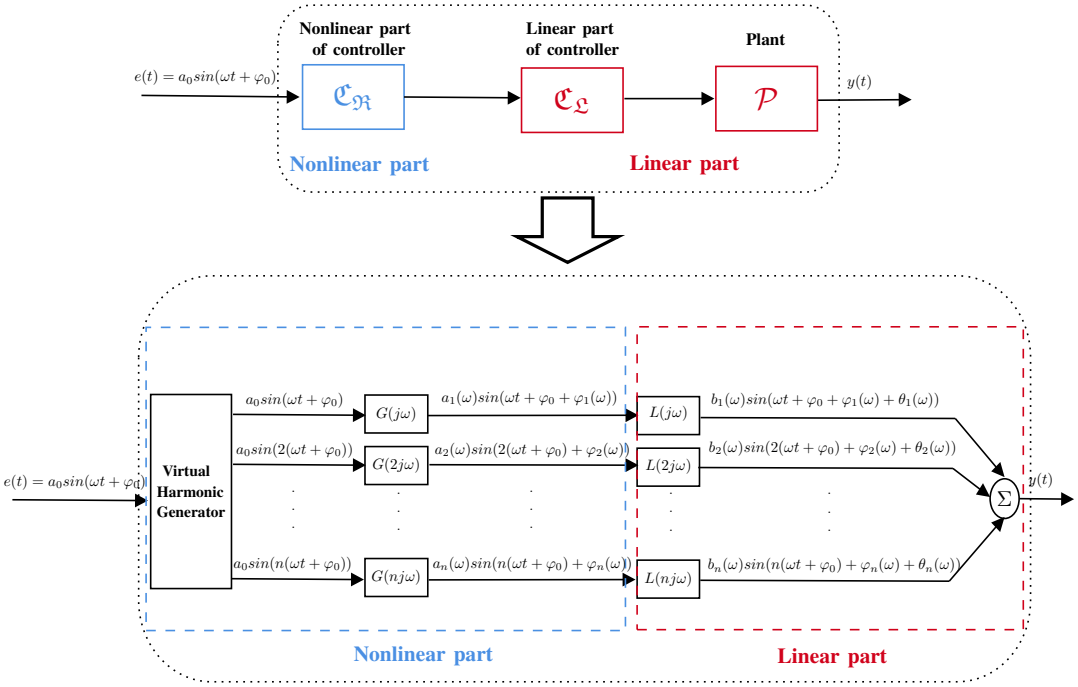

Fig. 1: HOSIDOFs Representation

Where

$$\Theta_\rho = \frac{2}{\pi}(I + e^{\frac{\pi A_r}{\omega}})(\frac{I - A_\rho}{I + A_\rho e^{\frac{\pi A_r}{\omega}}})((\frac{A_r}{\omega})^2 + I)^{-1}$$

In addition, HOSIDOFs for general reset elements are obtained in [22] as: $G(nj\omega) =$

$$\begin{cases} C_r(j\omega I - A_r)^{-1}(I + j\Theta_\rho(\omega))B_r + D_r & \text{for } n = 1 \\ C_r(j\omega n I - A_r)^{-1} j\Theta_\rho(\omega) B_r & \text{for } odd\ n \geq 2 \\ 0 & \text{for } even\ n \geq 2 \end{cases} \tag{3}$$

B. New Sensitivity Function

In linear systems, tracking error is obtained through sensitivity function which is defined as:

$$\frac{e}{r} = S(j\omega) = \frac{1}{1 + CG(j\omega)} \tag{4}$$

where $CG(j\omega)$ is the open loop transfer function of the whole linear system.

In order to get sensitivity function of nonlinear systems, describing function should be used for calculating $CG(j\omega)$. However, describing function only consider the first order harmonic which is inaccurate. To take into account the influence of high order harmonics, considering a sinusoidal input $r = Rsin(\omega t)$, it is defined a new sensitivity function for nonlinear systems as:

$$S_\partial(\omega) = \frac{\max(|e(t)|)}{|R|} \qquad \text{for } t \geq t_{ss} \tag{5}$$

where t_{ss} is the time when error becomes steady and periodic. Since $\max(|e(t)|)$ is the summation error of all order harmonics, from precision perspective, this new sensitivity function is more reliable than (4) and will be used in closed-loop performance analysis.

C. Shaping Filter

In the closed-loop system, the influence of noise can not be omitted. Especially when we put lead filter in front of the reset element, noise will first be amplified and then go through the reset element. It can be foresaw that these amplified noise will influence zero cross instants significantly when reaches certain magnitude which affect the performance. To reduce the influence of noise, a shaping filter $\mathfrak{C}_s$ is proposed within the reset element part at the reset branch as shown in Fig. 2.

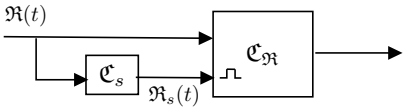

Fig. 2: Structure of shaping filter

This shaping filter consists of a low pass filter(LPF) and a tamed lead filter. It is represented as:

$$\mathfrak{C}_s = \underbrace{\left(\frac{1}{1 + \frac{s}{\omega_f}}\right)}_{LPF} \underbrace{\left(\frac{1 + \frac{s}{\omega_c/a}}{1 + \frac{s}{\omega_c a}}\right)}_{Lead} \tag{6}$$

where ω_f is the corner frequency of the LPF; ω_c is the bandwidth.

The LPF plays a role of decreasing the magnitude of noise. To make sure this additional shaping filter does not change the phase margin of the whole system, the tamed lead filter is used to compensate the phase change at bandwidth caused by the LPF.

The phase of LPF at bandwidth can be calculated by:

$$\phi_c = -tan^{-1}(\frac{\omega_c}{\omega_f}) \tag{7}$$

To compensate this phase change, the constant a is tuned as:

$$[tan^{-1}(a) - tan^{-1}(\frac{1}{a})] = -\phi_c \tag{8}$$

Smaller ω_f can filter out more noise, but it also corresponds to a large constant a, which means higher magnitude peak created by the lead filter. To trade off these two parameters, the corner frequency of LPF is tuning as $\omega_f = 2\omega_c$, with the corresponding $a = 1.62$.

Considering the phase of this shaping filter as $\phi(\omega)$, the HOSIDOFs of the reset element with shaping filter is recalculated according to the similar process in [9] and [22] as: $G_s(nj\omega) =$

$$\begin{cases} C_r(j\omega I - A_r)^{-1}(I + e^{j\phi}j\Theta_s(\omega))B_r + D_r & \text{for } n = 1 \\ C_r(j\omega nI - A_r)^{-1}e^{j\phi}j\Theta_s(\omega)B_r & \text{for } odd\ n \geq 2 \\ 0 & \text{for } even\ n \geq 2 \end{cases} \tag{9}$$

Where

$$\Theta_s = \Theta_\rho(\frac{-A_r sin\phi + \omega cos\phi I}{\omega})$$

III. Methodology

In linear controllers, different sequences of controller parts generate the same transfer function. However, when a reset element is applied in the system, performances of the system can be different depending on the relative sequence. Therefore, HOSIDFs tool is used to investigate and compare the magnitude of high order harmonics at different sequences.

For the general case, considering a combination of a linear part and a nonlinear reset part, the linear part can be divided into lag and lead elements. The transfer function of general linear lead and lag elements can be described as:

$$\mathfrak{C}_{lead}(s) = c_m s^m + c_{m-1}s^{m-1} + ... + c_0 s^0 \tag{10}$$

and

$$\mathfrak{C}_{lag}(s) = \frac{1}{d_p s^p + d_{p-1}s^{p-1} + ... + d_0 s^0} \tag{11}$$

There are 6 different sequences for three controller parts. However, when linear lag and lead elements are adjacent, changing their sequence doesn't make any difference. Therefore, 4 relevant sequences out of 6 are achieved in TABLE I.

TABLE I: Different configurations of genral case

No.	Sequence	Magnitude of the nth order harmonic
1	Lead-Reset-Lag	$\lvert\mathfrak{C}_{lead}(j\omega) \times G(nj\omega) \times \mathfrak{C}_{lag}(nj\omega)\rvert$
2	Lag-Reset-Lead	$\lvert\mathfrak{C}_{lag}(j\omega) \times G(nj\omega) \times \mathfrak{C}_{lead}(nj\omega)\rvert$
3	Reset-Lead-Lag	$\lvert G(nj\omega) \times \mathfrak{C}_{lead}(nj\omega) \times \mathfrak{C}_{lag}(nj\omega)\rvert$
4	Lead-Lag-Reset	$\lvert\mathfrak{C}_{lead}(j\omega) \times \mathfrak{C}_{lag}(j\omega) \times G(nj\omega)\rvert$

For the first order harmonic (n=1), DFs for all 4 configurations are the same. When it comes to high order harmonics, since lead filter has an increasing function of frequency and lag filter has a descending function of frequency, it is obvious that the first sequence has the smallest magnitude of high order harmonics.

For a simple example, if we combine a FORE with a first order lead filter: $1 + \frac{s}{\omega_d}$ and a first order lag filter: $1 + \frac{\omega_i}{s}$, the magnitude of the third order harmonic for four different sequences is visualized in Fig. 3.

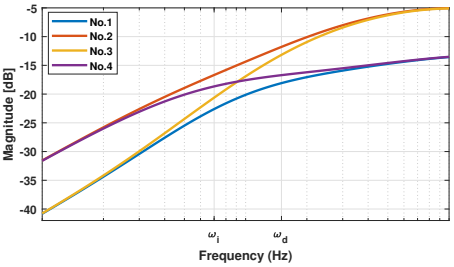

Fig. 3: The magnitude of the third order harmonic for different sequences of FORE

It is clear that before ω_i, the lag filter plays a role so that $No.1$ and $No.3$ have smaller magnitude of high order harmonics. After ω_d, lag filter has been terminated and lead filter comes into play, therefore $No.1$ and $No.4$ become smaller. In all range of frequencies, the first sequence always has the smallest magnitude and the second one has the largest amplitude of high order harmonics. The other two are the trade off between the first and second configurations. For higher order harmonics, this difference is increased.

IV. Closed-loop performance

Now, we find the optimal sequence which is Lead-Reset-Lag theoretically in the open-loop configuration. In order to investigate closed-loop performance of different sequences, a Lorentz-actuated precision positioning stage is used.

A. System Overview

As shown in Fig. 4, this system is guided using flexure cross hinge and actuated by a Visaton FR10-4 loudspeaker. With a Mercury 2000 reflective linear encoder, the horizontal position of the stage is achieved with a resolution of 100nm. The controllers are compiled using FPGA module and implemented via compact RIO real-time hardware.

Fig. 5 shows the frequency response of the system. This system is identified as a second order mass-spring-damper system with the transfer function:

$$P(s) = \frac{1}{1.077 \times 10^{-4}s^2 + 0.0049s + 4.2218} \tag{12}$$

B. Controller Design

For controlling this system, a Proportional Integration (PI)+Constant gain Lead phase (CgLp) compensator used.

CgLp element is made up by a reset filter and a corresponding linear lead filter as proposed in [24]. Consider a first order reset element $FORE$ and a linear lead part D as given below:

$$FORE(s) = \frac{1}{\not{s/\omega_r + 1}^{\gamma}} \tag{13}$$

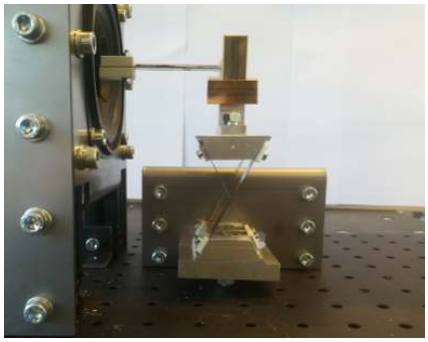

Fig. 4: Picture of precision positioning stage actuated by a loud speaker at the left

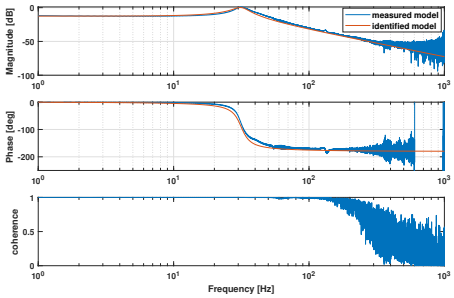

Fig. 5: Frequency response and the identified model

and

$$D(s) = \frac{s/\omega_d + 1}{s/\omega_t + 1} \tag{14}$$

where ω_r is the corner frequency of reset element, γ is the reset value, ω_d and ω_t are starting and taming frequencies of linear lead filter. By tuning $\omega_r = \omega_d/\alpha$, where α is a correction factor chosen according to [24], broadband phase lead can be achieved in the range of $[\omega_d, \omega_t]$ with constant gain(based on DF) as shown in Fig. 6.

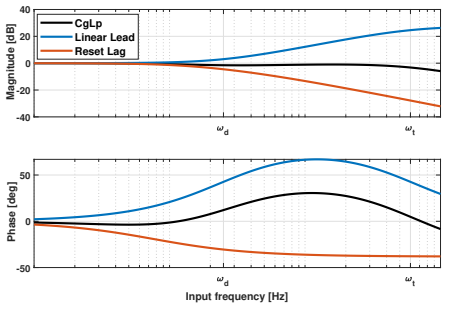

Fig. 6: DF of CgLp element

By replacing the D part of a traditional PID controller with a CgLp element, PI+CgLp controller is defined as:

$$\Sigma_{RC} = \underbrace{K_p\left(1+\frac{\omega_i}{s}\right)}_{PI}\underbrace{\left(\frac{1+\frac{s}{\omega_d}}{1+\frac{s}{\omega_t}}\right)\left(\frac{1}{s/\omega_r+1}\right)_{\gamma}}_{CgLp} \tag{15}$$

where ω_i is the corner frequency of the integrator element.

Considering the frequency response of the experimental setup, bandwidth is chosen as $\omega_c = 100Hz$ with 30 deg phase margin. According to the DF, ω_d is chosen to be $\omega_c/4$, ω_i=$\omega_c/10$ and ω_t=6ω_c. According to [24], correction factor α is taken as 1.62 so that $\omega_r = \omega_d/1.62$. Also, the reset value λ is selected as zero (classical reset). The tuning parameters of controller are listed in TABLE II.

TABLE II: Tuning parameters of CgLp+PI controller

symbol	parameter	Value
ω_c	bandwidth	100 Hz
ω_d	corner frequency of lead filter	25Hz
ω_t	taming frequency of lead filter	600 Hz
ω_r	corner frequency of reset lag filter	15.43 Hz
ω_i	corner frequency of integrator	10 Hz

A PI+CgLp consists of a lag element (PI), a lead element (D) and a reset element (FORE). Same as TABLE I, four relative sequences can be achieved. All four configurations have the same first order describing function as shown in Fig. 7.

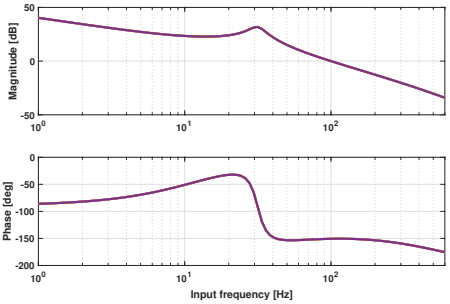

Fig. 7: DF of the whole system

C. Closed-loop Simulation: Sensitivity Function

The defined sensitivity function (5) of different configurations are used to compare their closed loop tracking performance. Disturbance and white noise will be added to mimic more realistic stimulation as shown in Fig. 8. Control elements are discretized with sampling frequency of 20 KHz. A disturbance signal between $0.5Hz$ and $30Hz$ which can cause 10% positioning deviation is applied for all configurations to mimic floor vibration.

By inputting sinusoidal reference signal at different frequencies, the steady value of $\max(|e(t)|)$ was recorded and used to plot $S_\partial(\omega)$ under different levels of noise as shown in Fig. 9. The sensitivity function according to DF is also plotted to show it is unreliable in nonlinear systems.

Firstly, the configuration Lead-Reset-Lag has the smallest $S_\partial(\omega)$ at all frequencies when the magnitude of noise signal is smaller than 0.5% of reference. In addition, when the

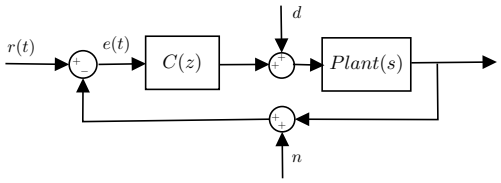

Fig. 8: Block diagram of close loop

magnitude of noise is bigger than 0.5%, the performances of configuration 1 and 4 deteriorate obviously at low frequencies while the configuration 2 and 3 do not change a lot. As we predicted, this kind of deterioration only occurs in the configurations with lead filter in front of the reset element. When the frequency of sinusoidal reference signal is bigger than ω_d (25Hz), the reference signal will also be amplified by the Lead filter, which cancels out the influence of noise. That's why this deterioration only appears at low frequencies.

D. Closed-loop Simulation: Control Output

By inputting sinusoidal reference signal at different frequencies, the maximum steady control output can also be recorded. Since the level of noise does not have much effect on control output, the control output with 0.1% noise is shown in Fig. 10 to illustrate the general result.

It is clear that configuration 2 and 3 have much larger control output comparing with others. This is because these two structures both have differentiator (Lead) after reset element. In these configurations, the 'jump' signal will first be generated by reset action, and then be differentiated consequently. The derivative of the 'jump' signal leads to large control output. Obviously, too much control output is not desired in reality since it can cause the saturation of controllers and even the instability of the system.

E. Closed-loop simulation: Effect of Shaping Filter

To attenuate the influence of noise at low frequencies, the shaping filter (6) is applied on configuration 1 and 4. For this system, ω_f is tuned as $2\omega_c = 200Hz$, with the corresponding $a = 1.62$.

The first and third order DFs of the original FORE and the FORE with shaping filter are shown in Fig. 11. It can be seen that the shaping filter does not change the DF so much, but the magnitude of the third order harmonic becomes smaller after ω_f.

With 3% noise in the system, Fig. 12 shows the sensitivity function when the shaping filter is applied on configuration 1 and 4. With the shaping filter, configuration 1 has the smallest sensitivity function again at almost all frequencies before bandwidth. Although the performance deteriorates a bit around bandwidth, it will not affect the tracking performance of trajectory signals [25] in reality where high frequency components are often pre-filtered out. Simulation has also been done for the situation when noise is larger than 3%, the results show 3% of noise is the maximum level this shaping filter can handle. For larger level of noise, shaping filter with smaller ω_f need to be used.

Above all, the configuration 1 is the optimal sequence for tracking performance when noise signal is not bigger than 0.5% amplitude of reference. For larger noise, the tracking performance will deteriorate at low frequencies. By adding the shaping filter as proposed above, the effect of noise can be attenuated and the suggested sequence still has the best performance until the level of noise reaches 3%.

F. Closed-loop simulation: Step Response

The step responses of different configurations are shown in Fig. 13. It can been seen that the steady state error only occurs when integrator (Lag) is in front of reset element. Overshoot occurs when differentiator (Lead) is located after reset element. Although, putting the lead filter after reset element has less rise time than Lead-Reset sequence, both configurations have the same settling time. All in all, Lead-Reset-Lag is also the optimal sequence.

V. Experimental validation

A series of experiments are conducted for configurations in TABLE I to check the simulation results and the optimal sequence. Since it is time consuming to plot the above sensitivity function in experiment, validation is only conducted in several specified frequencies. To avoid saturation, different magnitude of sinusoidal reference signals are applied at different frequencies as shown in TABLE III. The maximum steady error signal($\max(|e(t)|)$) and maximum steady digital control output are recorded in TABLE IV and TABLE V.

TABLE III: Magnitude of sinusoidal reference and the level of noise

Reference signal		level of noise
Frequency(Hz)	Magnitude $(0.1\mu m)$	Percentage
1	100	1%
5	120	0.83%
10	120	0.83%
15	150	0.67%
20	200	0.5%

TABLE IV: Maximum steady error of four different configurations

Reference	$\max(\|e(t)\|)$ $(0.1\mu m)$			
(Hz)	No.1	No.2	No.3	No.4
1	15	73	14	15
5	37	78	56	40
10	42	73	67	48
15	54	84	86	54
20	55	97	86	55

TABLE V: Maximum steady control output of four different configurations

Reference	Digital control output (count)			
(Hz)	No.1	No.2	No.3	No.4
1	486	26173	3103	1222
5	884	26806	12785	1513
10	941	24476	16972	1306
15	1364	25718	19539	1473
20	1677	27541	22038	1471

As shown in TABLE IV, configuration 1 has the smallest steady maximum error at almost all frequencies we tested. The only exception occurs at 1Hz, in which configuration 3

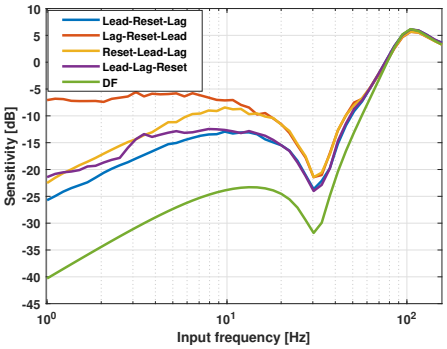

(a) Sensitivity function with 0.1% noise

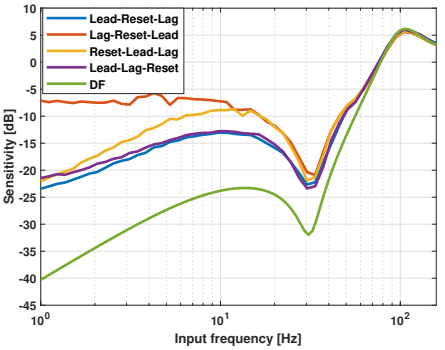

(b) Sensitivity function with 0.5% noise

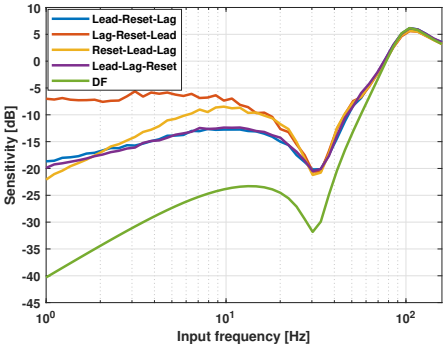

(c) Sensitivity function with 1% noise

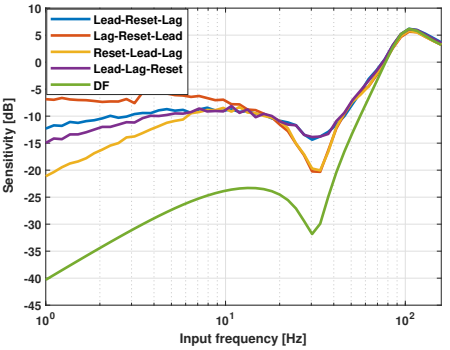

(d) Sensitivity function with 3% noise

Fig. 9: Sensitivity function with different level of noise

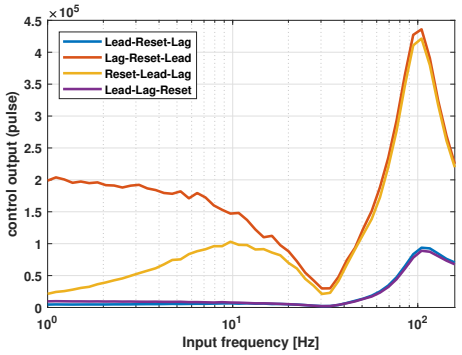

Fig. 10: Maximum steady control output with 0.1% noise

has the best tracking performance. This is consistent with the simulation results, since the noise level at 1Hz is 1%, noise tends to domain the performance. In addition, at $15Hz$ and $20Hz$ which are both more than ω_i, the effect of integrator is terminated, therefore configurations 1 and 4 have same performance.

From TABLE V, the control outputs of configuration 2 and 3 are much larger than configuration 1 and 4, which is consistent with the simulation.

To check the effect of noise at low frequencies more clearly, another set of experiments have been done at 1Hz with 3% noise. Since configuration 2 is the worst sequence in both tracking performance and saturation in previous experiments, only the other three configurations are compared in TABLE VI.

Without the shaping filter, we can see that the performance of No.1 and No.4 deteriorate seriously while the performance of configuration.3 does not change a lot as the level of noise increasing from 1% to 3%. When we apply the shaping filter, the performances of configuration 1 and 4 are improved significantly which means the effect of noise is effectively suppressed. With this kind of shaping filter, configuration 1 can perform well at low frequencies even with 3% noise.

TABLE VI: Influence of shaping filter for maximum steady error

Configuration	level of noise	$\max(\lvert e(t)\rvert)$ $(0.1\mu m)$		
		No.1	No.3	No.4
without shaping filter	1%	15	14	15
without shaping filter	3%	49	20	32
with shaping filter	3%	19	19	21

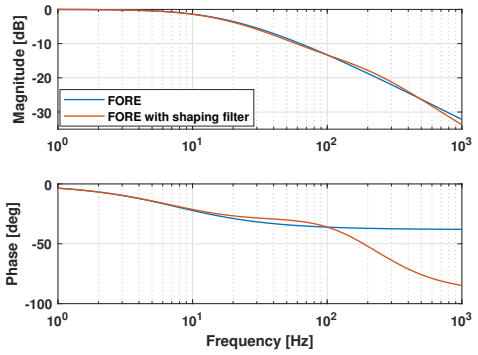

(a) The first order DFs

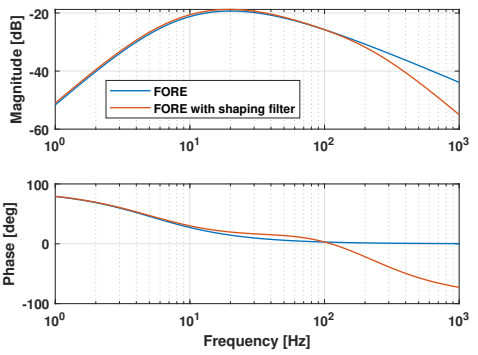

(b) The third order DFs

Fig. 11: The first and third order DFs of FORE and FORE with shaping filter

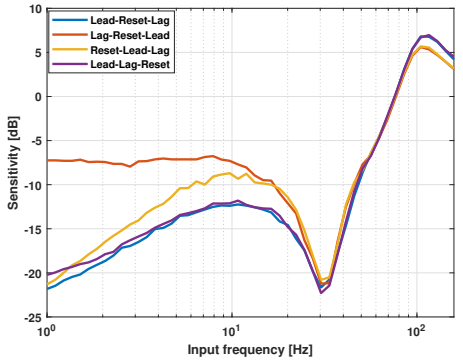

Fig. 12: Sensitivity function with 3% noise when shaping filter is applied on configuration 1 and 4

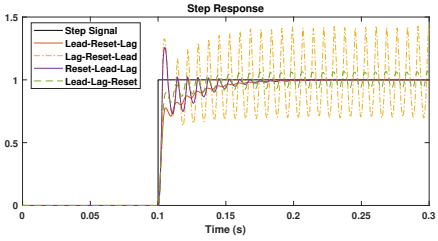

Fig. 13: Step responses of different configurations

VI. Conclusion

This paper has proposed an optimized strategy to arrange the sequence of controller parts when a reset element is used. Firstly, the performances of different sequences were investigated by considering high order harmonics using HOSIDFs theory. The optimal sequence in which the magnitude of high order harmonics is minimum is achieved. Next, the closed loop performances of a high-tech positioning stage with PI+CgLp controller were analyzed in both simulation and experiment for different sequences of controller parts. The results illustrated that when the magnitude of noise within the system is smaller than 0.5% of the reference signal, it is safe to say the suggested sequence has the best performance; otherwise, the performance of the suggested sequence will deteriorate at low frequencies. In this case, a shaping filter was proposed to deal with the problem. It is revealed that this shaping filter attenuated the influence of noise successfully and make the suggested sequence have the best tracking performance with up to 3% noise. In addition, the suggested sequence also has the smallest control output, which means from the perspective of actuator saturating in reality, it is also the optimal sequence.

Above all, this paper suggests the optimal sequence for different parts of a controller which has a reset element to achieve high precision and has minimum controller output. The results can facilitate the use of reset controllers in a broad range of applications in high-tech industry. For further studies, applying this approach on other kinds of nonlinear controllers to increase their performance is a promising topic.

References

[1] S. Skogestad and I. Postlethwaite, *Multivariable feedback control: analysis and design*. Wiley New York, 2007, vol. 2.

[2] R. M. Schmidt, G. Schitter, and A. Rankers, *The Design of High Performance Mechatronics-: High-Tech Functionality by Multidisciplinary System Integration*. Ios Press, 2014.

[3] L. Chen, N. Saikumar, S. Baldi, and S. H. HosseinNia, "Beyond the waterbed effect: Development of fractional order crone control with non-linear reset," in *2018 Annual American Control Conference (ACC)*. IEEE, 2018, pp. 545–552.

[4] M. Zarghami and S. HassanHosseinNia, "Fractional order set point regulator using reset control: Application to egr systems," in *Proceedings of the 2017 The 5th International Conference on Control, Mechatronics and Automation*. ACM, 2017, pp. 35–41.

[5] S. H. HosseinNia, I. Tejado, and B. M. Vinagre, "Basic properties and stability of fractional-order reset control systems," in *2013 European Control Conference (ECC)*. IEEE, 2013, pp. 1687–1692.

[6] ——, "Fractional-order reset control: Application to a servomotor," *Mechatronics*, vol. 23, no. 7, pp. 781–788, 2013.

[7] L. Marinangeli, F. Alijani, and S. H. HosseinNia, "Fractional-order positive position feedback compensator for active vibration control of a smart composite plate," *Journal of Sound and Vibration*, vol. 412, pp. 1–16, 2018.

[8] J. Clegg, "A nonlinear integrator for servomechanisms," *Transactions of the American Institute of Electrical Engineers, Part II: Applications and Industry*, vol. 77, no. 1, pp. 41–42, 1958.

[9] Y. Guo, Y. Wang, and L. Xie, "Frequency-domain properties of reset systems with application in hard-disk-drive systems," *IEEE Transactions on Control Systems Technology*, vol. 17, no. 6, pp. 1446–1453, 2009.

[10] I. Horowitz and P. Rosenbaum, "Non-linear design for cost of feedback reduction in systems with large parameter uncertainty," *International Journal of Control*, vol. 21, no. 6, pp. 977–1001, 1975.

[11] L. Hazeleger, M. Heertjes, and H. Nijmeijer, "Second-order reset elements for stage control design," in *2016 American Control Conference (ACC)*. IEEE, 2016, pp. 2643–2648.

[12] J. Zheng, Y. Guo, M. Fu, Y. Wang, and L. Xie, "Development of an extended reset controller and its experimental demonstration," *IET Control Theory & Applications*, vol. 2, no. 10, pp. 866–874, 2008.

[13] A. Baños and A. Vidal, "Definition and tuning of a pi+ ci reset controller," in *2007 European Control Conference (ECC)*. IEEE, 2007, pp. 4792–4798.

[14] A. Barreiro, A. Baños, S. Dormido, and J. A. González-Prieto, "Reset control systems with reset band: Well-posedness, limit cycles and stability analysis," *Systems & Control Letters*, vol. 63, pp. 1–11, 2014.

[15] J. Zheng, Y. Guo, M. Fu, Y. Wang, and L. Xie, "Improved reset control design for a pzt positioning stage," in *2007 IEEE International Conference on Control Applications*. IEEE, 2007, pp. 1272–1277.

[16] Y. Li, G. Guo, and Y. Wang, "Reset control for midfrequency narrowband disturbance rejection with an application in hard disk drives," *IEEE Transactions on Control Systems Technology*, vol. 19, no. 6, pp. 1339–1348, 2011.

[17] H. Li, C. Du, and Y. Wang, "Discrete-time h 2 optimal reset control with application to hdd track-following," in *2009 Chinese Control and Decision Conference*. IEEE, 2009, pp. 3613–3617.

[18] ——, "Optimal reset control for a dual-stage actuator system in hdds," *IEEE/ASME Transactions on Mechatronics*, vol. 16, no. 3, pp. 480–488, 2011.

[19] Y. Li, G. Guo, and Y. Wang, "Phase lead reset control design with an application to hdd servo systems," in *2006 9th International Conference on Control, Automation, Robotics and Vision*. IEEE, 2006, pp. 1–6.

[20] D. Wu, G. Guo, and Y. Wang, "Reset integral-derivative control for hdd servo systems," *IEEE Transactions on Control Systems Technology*, vol. 15, no. 1, pp. 161–167, 2007.

[21] P. Nuij, O. Bosgra, and M. Steinbuch, "Higher-order sinusoidal input describing functions for the analysis of non-linear systems with harmonic responses," *Mechanical Systems and Signal Processing*, vol. 20, no. 8, pp. 1883–1904, 2006.

[22] K. Heinen, "Frequency analysis of reset systems containing a clegg integrator: An introduction to higher order sinusoidal input describing functions," 2018.

[23] A. Baños and A. Barreiro, *Reset control systems*. Springer Science & Business Media, 2011.

[24] N. Saikumar, R. Sinha, and S. H. Hoseinnia, "constant in gain lead in phaseelement-application in precision motion control," *IEEE/ASME Transactions on Mechatronics*, 2019.

[25] P. Lambrechts, M. Boerlage, and M. Steinbuch, "Trajectory planning and feedforward design for electromechanical motion systems," *Control Engineering Practice*, vol. 13, no. 2, pp. 145–157, 2005.

5

Conclusion

The objective of this thesis was established as follow:

Find the optimal sequence for reset controllers which has the smallest magnitude of high order harmonics and check if this sequence has the best performance in closed loop.

Firstly, an introduction about reset control was given in the literature review part. Although reset controllers can be used to overcome the limitation of linear controllers, high order harmonics are introduced into the system because of non-linearity which deteriorate the performance of the system. Therefore, it is necessary to reduce the magnitude of high order harmonics as much as possible.

Then, by using HOSIDOFs tool, it is found that the sequence of different parts of a reset controller has effect on the magnitude of high order harmonics. Based on the HOSIDOFs theory, the optimal sequence of open loop in which the magnitude of high order harmonics is minimum is achieved for a general reset controller.

Finally, the closed loop performances of a high-tech positioning stage with PI+CgLp controller were analyzed in both simulation and experiment for different sequences of controller parts. The results show that:

- From the step response perspective, the suggested sequence (Lead-Reset-Lag) has the smallest settling time among all sequences without steady state error and overshoot.
- From the precision perspective, when the magnitude of noise within the system is smaller than 0.5% of the reference signal, it is safe to say the suggested sequence (Lead-Reset-Lag) has the best precision performance. When the magnitude of noise within the system is bigger than 0.5%, the performance of the suggested sequence (Lead-Reset-Lag) deteriorates at low frequencies.
- From the perspective of controller's saturation, the suggested sequence (Lead-Reset-Lag) has the smallest control output.

To deal with the performance deterioration at low frequencies because of high level noise, two different types of shaping filters were proposed in appendix C:

- Type 1: Use a LPF to filter out noise and a tamed lead filter to compensate the phase change at bandwidth.
- Type 2: Use a LPF to filter out noise and change reset value γ to compensate the phase change at bandwidth.

The HOSIDOFs of a reset element with shaping filter were derived in appendix B to facilitate the tuning and analysis of the shaping filter. The simulation and experiment results show that both types of shaping filters have similar effect to make the suggested sequence (Lead-Reset-Lag) have the best performance with up to 3% noise. Comparatively speaking, the tuning rule of the Type 1 shaping filter is simpler and more general than Type 2, therefore is a better choice.

In appendix D, a fourth order trajectory was applied for different sequences to check their tracking performance in simulation. The results show that the suggested sequence has the smallest maximum tracking error when there is no noise within the system. The deterioration occurs when the level of noise increases. After applying the shaping filter, the suggested sequence achieced the best precision performance with up to 3% noise.

In appendix E, a different kind of shaping filter was attempted to get less phase lag. Although the phase lag was reduced in that case, the additional shaping filter also increased the high order harmonics, more investigations need to be done in that field.

Following are the recommendations for further studies:

- This work focused on finding the optimal sequence for reset controllers. However, the theory of HOSIDOFs holds for all non-linear controllers. Applying this optimal sequence on other kinds of nonlinear controllers to increase their performance can be a promising direction.
- Although the proposed shaping filter attenuates the influence of noise to some extent, the maximum level of noise it can deal with is around 3%. Further research need to be done to find more effective way to handle the deterioration because of noise.

A

HOSIDOFs of Different Sequences

This appendix elaborates the HOSIDOFs of different sequences according to block diagrams, followed by an illustrative example.

A.1. The optimal sequence in open loop

First consider an open loop consists of a linear filter ($\mathfrak{C}_{\mathcal{L}}$) and a nonlinear reset filter ($\mathfrak{C}_{\Re}$). The block diagrams of HOSIDOFs for two different sequences are shown in Fig. A.1. For the first sequence, when the nonlinear part is in front of the linear part, the magnitude of the nth order harmonic is:

$$b_n(\omega) = |G(nj\omega)L(nj\omega)|$$

where G(s) is the HOSIDOFs of the nonlinear part and L(s) is the transfer function of the linear part.

For the second sequence, when the linear part is in front of the nonlinear part, the magnitude of the nth order harmonic becomes:

$$b_n(\omega) = |L(j\omega)G(nj\omega)|$$

To reduce the magnitude of high order harmonics as much as possible, the following ***Lemma*** can be derived:

If the linear filter is a descending function of frequency, then it has to be located after the nonlinear element(Fig. A.1a), otherwise it should be located before that (Fig. A.1b).

A.2. Illustrative example

In this section, the HOSIDOFs of a Clegg integrator combining with a linear Differentiator with different sequences are compared as an illustrative example. Two different sequences are shown in Fig. A.2.

A

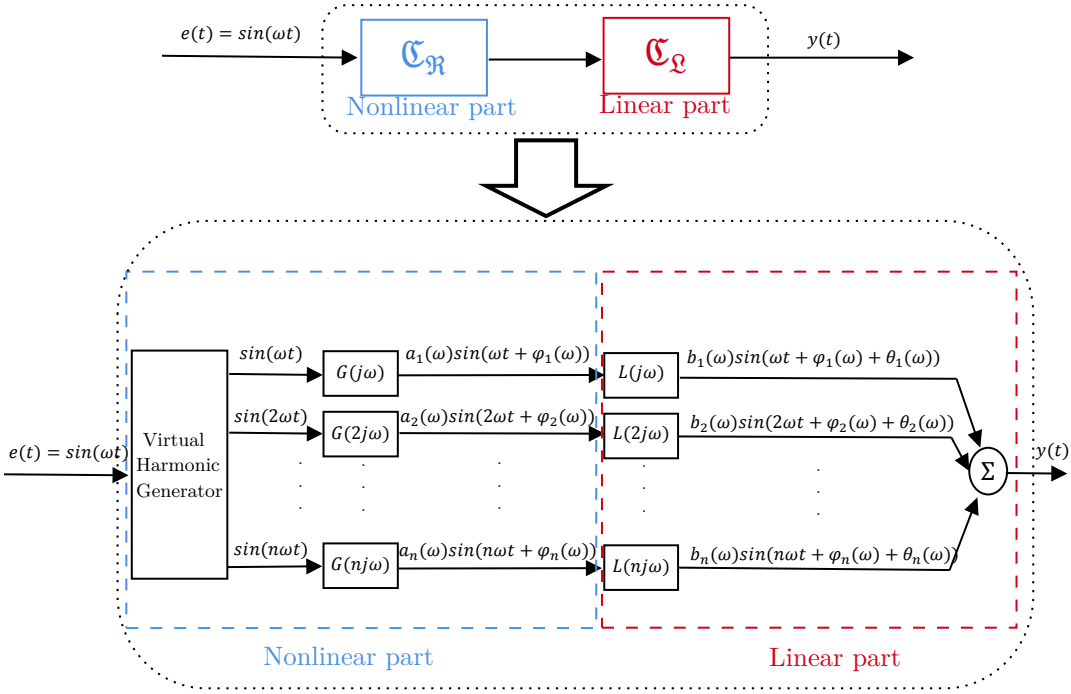

(a) HOSIDOFs when nonlinear part in front of linear part

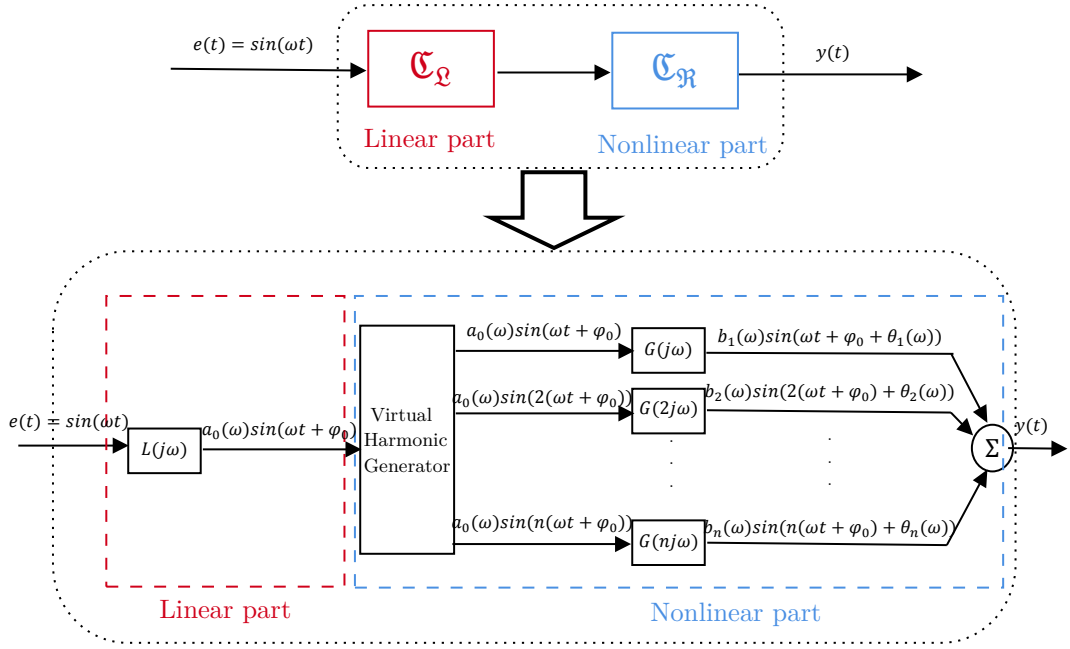

(b) HOSIDOFs when linear part in front of nonlinear part

Figure A.1: Block Diagram of HOSIDOFs

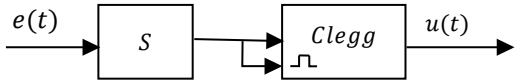

(a) First Differentiator, then Clegg

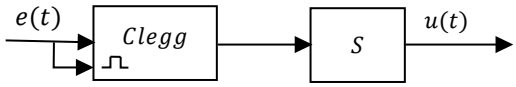

(b) First Clegg, then Differentiator

Figure A.2: Combination of Differentiator and Clegg

The HOSIDOFs of the first sequence is obtained as:

$$G_1(\omega,n)=\begin{cases}(1+j\frac{4}{\pi}) & \text{for } n=1\\ \frac{4j}{\pi n}(-1)^{\frac{n-1}{2}} & \text{for } odd\ n\geq 2\\ 0 & \text{for } even\ n\geq 2\end{cases} \tag{A.1}$$

The second sequence's HOSIDOFs is:

$$G_2(\omega,n)=\begin{cases}(1+j\frac{4}{\pi}) & \text{for } n=1\\ \frac{4j}{\pi} & \text{for } odd\ n\geq 2\\ 0 & \text{for } even\ n\geq 2\end{cases} \tag{A.2}$$

For a single Clegg integrator, the HOSIDFs becomes:

$$CI(\omega,n)=\begin{cases}\frac{1}{j\omega}(1+j\frac{4}{\pi}) & \text{for } n=1\\ \frac{4}{\pi\omega n} & \text{for } odd\ n\geq 2\\ 0 & \text{for } even\ n\geq 2\end{cases} \tag{A.3}$$

Compare (A.1), (A.2) and (A.3), the magnitude of high order harmonics for two different sequences can be represented as:

$$|G_1(\omega,n)|=|j\omega CI(\omega,n)|$$
$$|G_2(\omega,n)|=|CI(\omega,n)nj\omega|$$

It is clear that the first sequence generates the smaller magnitude of high order harmonics. Since the Differentiator element has an increasing function of frequency, put it in front of the nonlinear part is a better choice in open loop.

B

HOSIDOFs with Shaping Filter

This appendix provides the detail process of deriving the HOSIDOFs when we have a shaping filter in the reset branch.

For a reset element with shaping filter:

$$\Sigma_{Rs} = \begin{cases} \dot{x}_r(t) = A_r x_r(t) + B_r e(t) & \text{if } e_s(t) \neq 0 \\ x_r(t^+) = A_\rho x_r(t) & \text{if } e_s(t) = 0 \\ u(t) = C_r x_r(t) \end{cases} \tag{B.1}$$

The block diagram is shown in Fig. B.1.

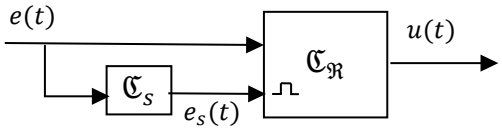

Figure B.1: Structure of shaping filter

Use the following well defined notations same as [12] for convenience:

$$\Lambda(\omega) \triangleq \omega^2 I + A_r^2$$
$$\Delta(\omega) \triangleq I + e^{\frac{\pi}{\omega}A_r}$$
$$\Delta_D(\omega) \triangleq I + A_\rho e^{\frac{\pi}{\omega}A_r}$$
$$\Gamma_D(\omega) = \Delta_D^{-1}(\omega) A_\rho \Delta(\omega) \Lambda^{-1}(\omega)$$

Consider sinusoidal excitation input

$$e(t) = sin(\omega t - \phi(\omega)) \tag{B.2}$$

where $\phi(\omega)$ is the phase of the shaping filter $\mathfrak{C}_s$. Therefore, the shaped signal becomes:

$$e_s(t) = sin(\omega t) \tag{B.3}$$

B

the set of the reset time instants is

$$t_k = \frac{k\pi}{\omega} \quad k = 0, 1, \ldots$$

Define $\eta_k = x\left(t_{2k}^+\right), \zeta_k = x\left(t_{2k+1}^+\right)$ and

$$\psi(t) \triangleq \int_0^t e^{-A_r s} B_r \sin(\omega s - \phi(\omega)) \mathrm{d}s \tag{B.4}$$

The solution of B.1 is given in [12] as:

$$x(t) = \begin{cases} e^{A(t-t_{2k})}\eta_k \\ +e^{At}\left[\psi(t) - \psi\left(t_{2k}\right)\right], \quad t \in (t_{2k}, t_{2k+1}] \\ e^{A(t-t_{2k+1})}\zeta_k \\ +e^{At}\left[\psi(t) - \psi\left(t_{2k+1}\right)\right], \quad t \in (t_{2k+1}, t_{2k+2}] \end{cases} \tag{B.5}$$

where

$$\lim_{k\to+\infty} \eta_k = -\Delta_D^{-1}(\omega) A_r e^{\frac{\pi}{\omega}A_r} \psi\left(\frac{\pi}{\omega}\right) \tag{B.6}$$

$$\lim_{k\to+\infty} \zeta_k = \Delta_D^{-1}(\omega) A_r e^{\frac{\pi}{\omega}A_r} \psi\left(\frac{\pi}{\omega}\right) \tag{B.7}$$

The response of the system can be represented as:

$$u(t) = u_{ss}(t) + u_t(t)$$

where $u_{ss}(t)$ is the steady-state response and $u_t(t)$ is the transient response which dies away with time.

The HOSIDOFs of this system is defined in [15] by

$$G(nj\omega) = \frac{U_{\mathrm{ss}}(nj\omega)}{E(j\omega)} \tag{B.8}$$

where

$$U_{\mathrm{ss}}(nj\omega) = \frac{\omega}{2\pi}\int_0^{\frac{2\pi}{\omega}} u_{\mathrm{ss}}(t) e^{-nj\omega t} dt \tag{B.9}$$

$$E(j\omega) = \frac{\omega}{2\pi}\int_0^{\frac{2\pi}{\omega}} e(t) e^{-j\omega t} dt \tag{B.10}$$

By B.1, B.5, B.6, B.7, when $t \in (t_k, t_{k+1}]$

$$\begin{aligned} u_{\mathrm{ss}}(t) &= C_r e^{A_r t}\left\{(-1)^{k+1} e^{-A_r t_k}\Gamma_D(\omega)\left[-A_r sin\phi(\omega) + \omega cos\phi(\omega) I\right] B_r + \psi(t) - \psi\left(t_k\right)\right\} \\ &= C_r e^{A_r t}\theta_k(\omega) - C_r\Lambda^{-1}(\omega)[\omega I \cos(\omega t - \phi) + A_r \sin(\omega t - \phi)]B_r \end{aligned}$$

where

$$\theta_k(\omega) = (-1)^{k+1} e^{-A_r t_k}\left[\Gamma_D(\omega) - \Lambda^{-1}(\omega)\right]\left[-A_r sin\phi(\omega) + \omega cos\phi(\omega) I\right] B_r$$

The Fourier series of u_{ss} for n order harmonics is calculated as

$$\begin{aligned} U_{\mathrm{ss}}(nj\omega) &= \frac{\omega}{2\pi}\int_0^{\frac{2\pi}{\omega}} u_{\mathrm{ss}}(t)e^{-nj\omega t}\mathrm{d}t \\ &= \frac{\omega C_r}{2\pi}(I_1+I_2) - \frac{\omega C_r\Lambda^{-1}(\omega)}{2\pi}(\omega J_1 + AJ_2)B_r \end{aligned}$$

$$\begin{aligned} I_1 &= \int_0^{\frac{\pi}{\omega}} e^{A_r t}\theta_0(\omega)e^{-nj\omega t}\mathrm{d}t \\ &= (nj\omega I - A_r)^{-1}\Delta(\omega)\theta_0(\omega) \end{aligned}$$

$$\begin{aligned} I_2 &= \int_{\frac{\pi}{\omega}}^{\frac{2\pi}{\omega}} e^{A_r t}\theta_1(\omega)e^{-nj\omega t}\mathrm{d}t \\ &= -(nj\omega I - A_r)^{-1}\Delta(\omega)e^{\frac{\pi}{\omega}A_r}\theta_1(\omega) \end{aligned}$$

$$J_1 = \int_0^{\frac{2\pi}{\omega}} e^{-nj\omega t}\cos(\omega t-\phi)\mathrm{d}t = \begin{cases} \frac{\pi}{\omega}e^{-\phi j} & \text{if } n=1 \\ 0 & \text{if } n>1 \end{cases}$$

$$J_2 = \int_0^{\frac{2\pi}{\omega}} e^{-nj\omega t}\sin(\omega t-\phi)\mathrm{d}t = \begin{cases} -j\frac{\pi}{\omega}e^{-\phi j} & \text{if } n=1 \\ 0 & \text{if } n>1 \end{cases}$$

It is easy to get

$$E(j\omega) \triangleq \frac{\omega}{2\pi}\int_0^{\frac{2\pi}{\omega}} \sin(\omega t-\phi)e^{-j\omega t}\mathrm{d}t = -j\frac{e^{-j\phi}}{2}$$

From B.8

$$G_s(nj\omega) = \begin{cases} C_r(j\omega I - A_r)^{-1}(I + e^{j\phi}j\Theta_s(\omega))B_r & \text{for } n=1 \\ C_r(j\omega nI - A_r)^{-1}e^{j\phi}j\Theta_s(\omega)B_r & \text{for } odd\ n\geq 2 \\ 0 & \text{for } even\ n\geq 2 \end{cases} \tag{B.11}$$

Where

$$\Theta_s = -\frac{2\omega}{\pi}\Delta(\omega)\left[\Gamma_D(\omega) - \Lambda^{-1}(\omega)\right](-A_r sin\phi + \omega cos\phi I)$$

If the output function is replaced by

$$u(t) = C_r x_r(t) + D_r e(t) \tag{B.12}$$

The HOSIDOFs becomes

$$G_s(nj\omega) = \begin{cases} C_r(j\omega I - A_r)^{-1}(I + e^{j\phi}j\Theta_s(\omega))B_r + D_r & \text{for } n=1 \\ C_r(j\omega nI - A_r)^{-1}e^{j\phi}j\Theta_s(\omega)B_r & \text{for } odd\ n\geq 2 \\ 0 & \text{for } even\ n\geq 2 \end{cases} \tag{B.13}$$

Where

$$\Theta_s = -\frac{2\omega}{\pi}\Delta(\omega)\left[\Gamma_D(\omega) - \Lambda^{-1}(\omega)\right](-A_r sin\phi + \omega cos\phi I)$$

C

Shaping Filter for Noise Attenuation

In this appendix, two different types of shaping filters are applied to attenuate the influence of noise.

Type 1: Use a LPF to filter out noise and a tamed lead filter to compensate the phase change at bandwidth.

This shaping filter is represented as:

$$\mathfrak{C}_s = \underbrace{\left(\frac{1}{1+\frac{s}{\omega_f}}\right)}_{LPF}\underbrace{\left(\frac{1+\frac{s}{\omega_c/a}}{1+\frac{s}{\omega_c a}}\right)}_{Lead} \tag{C.1}$$

where ω_f is the corner frequency of the LPF, ω_c is the bandwidth and a is a constant.

The phase of LPF at bandwidth can be calculated by:

$$\phi_{lag} = -tan^{-1}(\frac{\omega_c}{\omega_f}) \tag{C.2}$$

To compensate this phase lag, the constant a is tuned as:

$$[tan^{-1}(a) - tan^{-1}(\frac{1}{a})] = -\phi_{lag} \tag{C.3}$$

Type 2: Use a LPF to filter out noise and change reset value γ to compensate the phase change at bandwidth.

The corresponding reset values γ for this system have been calculated according to $G_s(j\omega)$ for different ω_f as shown in Fig. C.1.

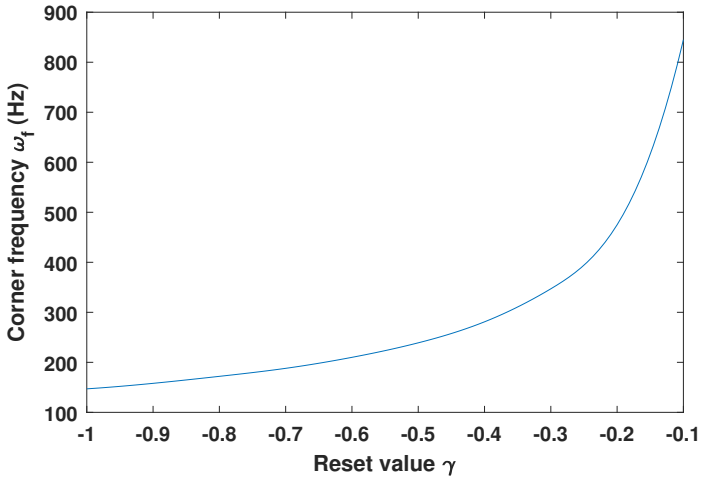

Figure C.1: corresponding reset value γ for different ω_f

With 3% noise, two types of shaping filters with different ω_f are applied on configuration 1 and 4. The new sensitivity functions are simulated and shown in Fig. C.2.

The results show that both types of shaping filters attenuate the influence of noise at low frequencies successfully and increase the performance of the suggested sequence. For the ***Type 1*** shaping filter, the optimal parameters are: $\omega_f 200Hz; a = 1.62$. For the ***Type 2*** shaping filter, the optimal parameters are: $\omega_f 300Hz; \gamma = -0.37$.

However, for different reset controllers, the corresponding reset value γ for different ω_f needs to be recalculated through HOSIDOFs which is not convenient. Comparatively speaking, the tuning rule of the ***Type 1*** shaping filter is more general for different controllers and can achieve similar effect with ***Type 2***.

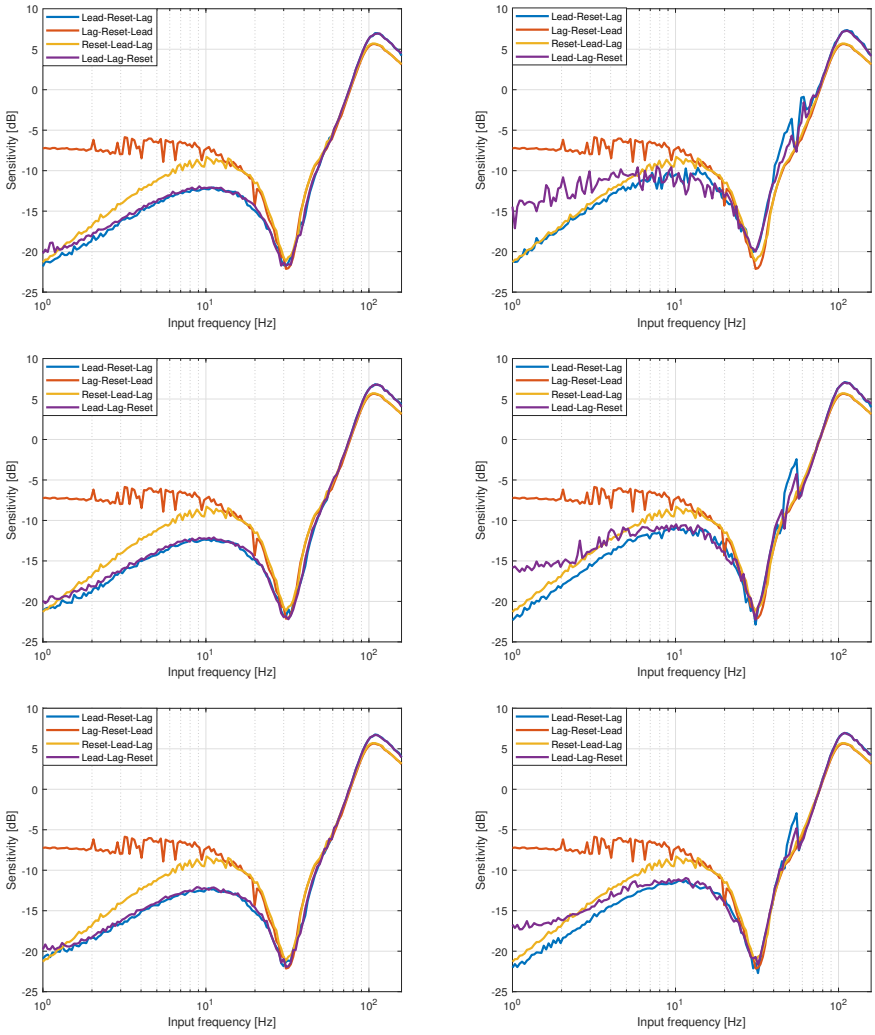

(a) The sensitivity functions when applying Type 1 shaping filter for configuration 1 and 4

(b) The sensitivity functions when applying Type 2 shaping filter for configuration 1 and 4

Figure C.2: Effect of two types of shaping filters with different ω_f

D

Trajectory Tracking Performance

In this appendix, a fourth order trajectory as explained in [17] was applied for reset controller with different sequences to check their tracking performance in simulation as shown in Fig. D.1.

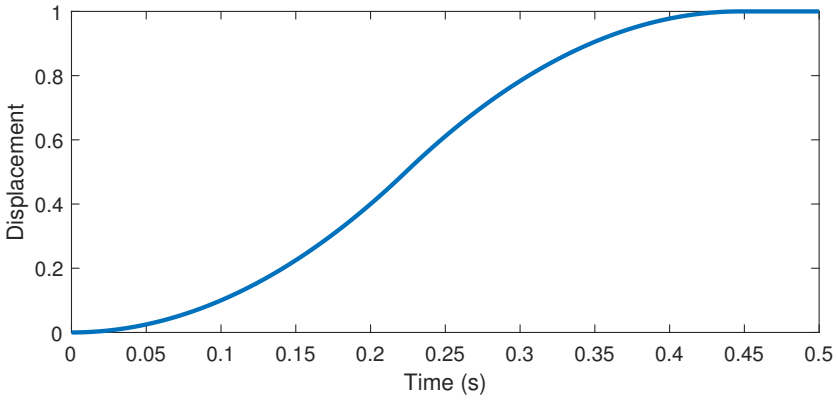

Figure D.1: Trajectory reference signal

Fig. D.2 shows the simulation result of the error signal of different sequences when there is no noise and 1% noise within the system respectively.

It can be seen that when there is no noise within the system, the suggested sequence (Lead-Reset-Lag) has the smallest maximum tracking error. However, when the noise level is 1%, the tracking error of the suggested sequence increases significantly.

To attenuate the deterioration because of noise, the proposed shaping filter in appendix C was applied on configurations 1 and 4 where the Lead filter is in front of the reset element. As shown in Fig. D.3, the shaping filter attenuates the influence of noise successfully and makes the suggested sequence have the smallest tracking error with up to 3% noise.

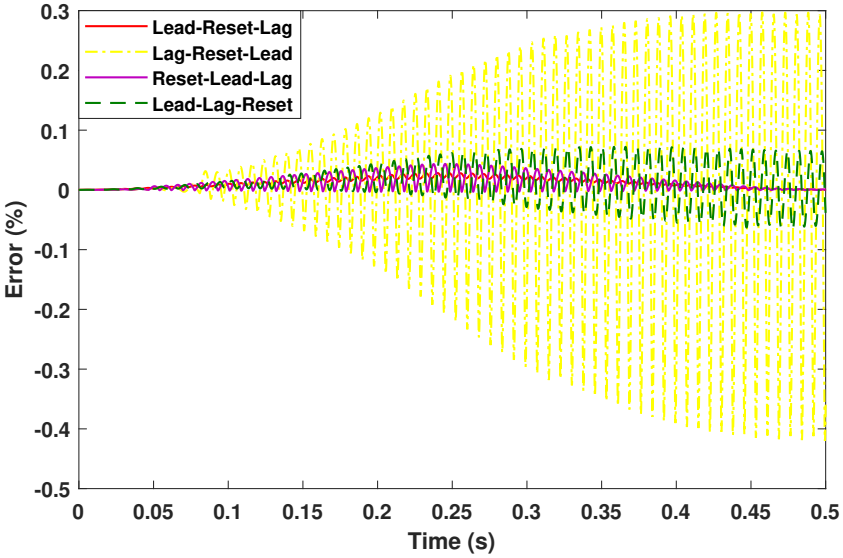

(a) The error signal of different configurations without noise

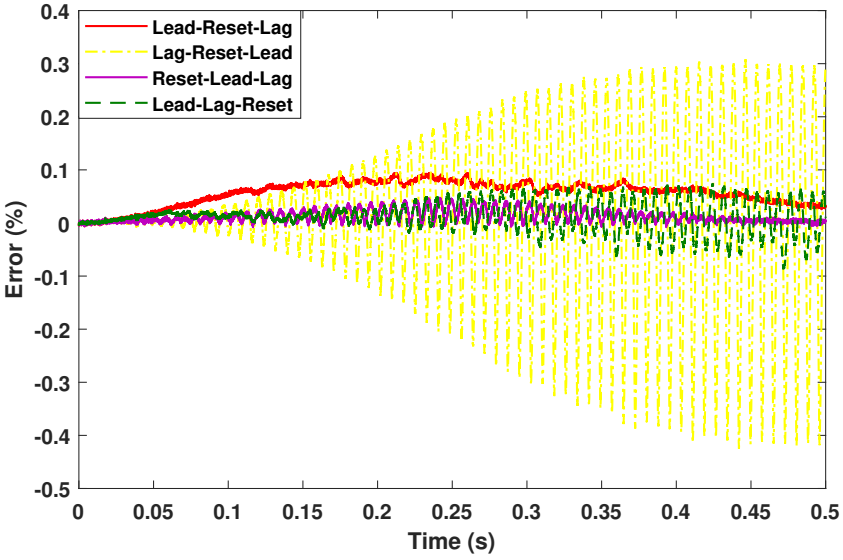

(b) The error signal of different configurations with 1% noise

Figure D.2: Trajectory tracking performance without shaping filter

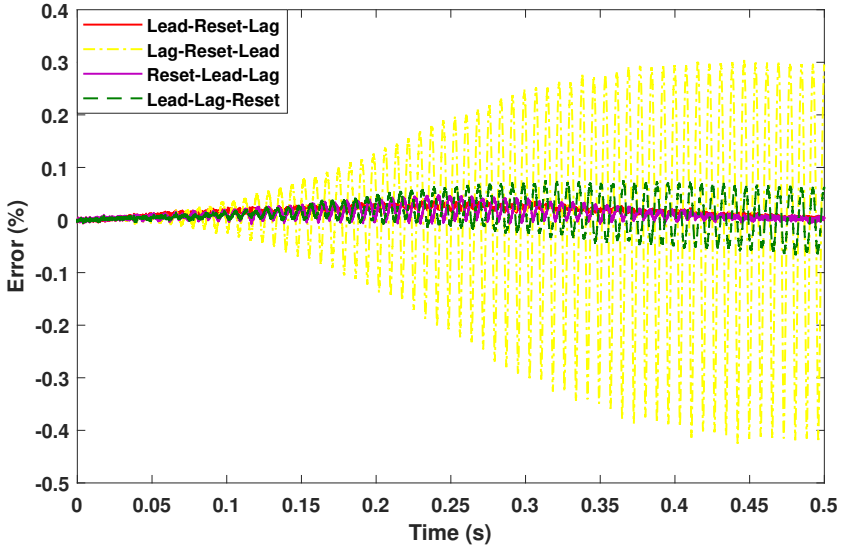

(a) The error signal of different configurations with 1% noise after applying shaping filter in configurations 1 and 4

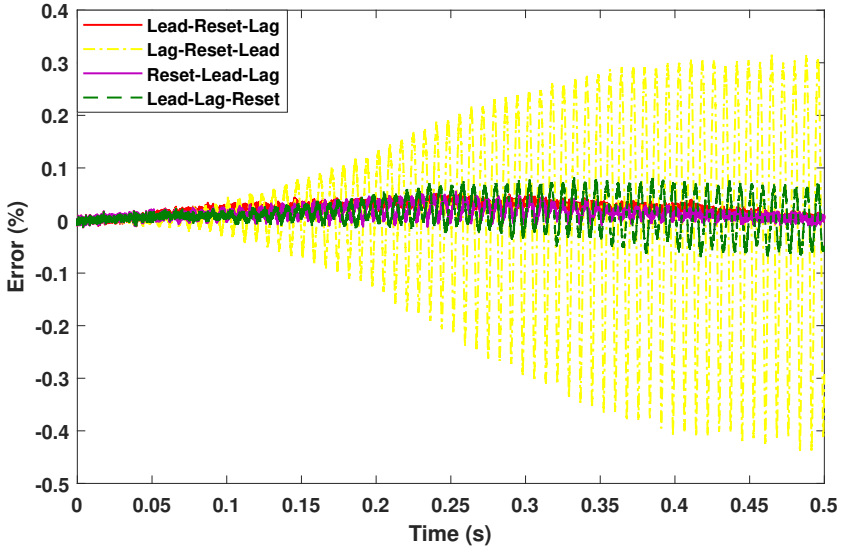

(b) The error signal of different configurations with 3% noise after applying shaping filter in configurations 1 and 4

Figure D.3: Trajectory tracking performance with shaping filter

E

Shaping Filter for Less Phase Lag

In this appendix, a shaping filter is applied to get less phase lag.

Consider the same structure as Fig. B.1 when a shaping filter is applied on a FORE with reset matrix $A_\rho = 0$. With excitation input $e(t) = sin(\omega t)$, a fractional order derivative is used as the shaping filter to generate the shaped signal $e_s(t) = sin(\omega t + \pi/4)$. By tuning the corner frequency, we make the FORE with the shaping filter have almost the same magnitude of the first order DF as the original FORE.

Fig. E.1 shows the first and third order DFs of the original FORE and the FORE with this shaping filter. Comparing with the original FORE, resetting according to $e_s(t) = sin(\omega t + \pi/4)$ generates less phase lag. However, the high order harmonics increase when we add this shaping filter.

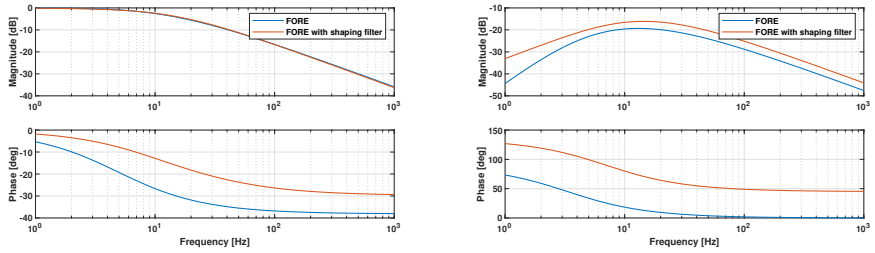

(a) The 1st order DFs (b) The 3rd order DFs

Figure E.1: Comparison of FORE and FORE with shaping filter

An alternative way to get less phase lag is by changing A_ρ to negative reset values. We tune the reset value to make the phase lag the same as the FORE with the shaping filter.

Fig. E.2 shows the first and third order DFs of the FORE with the shaping filter and the FORE with the negative reset value. It is clear that with the same magnitude and phase lag of the first order DF, using negative γ generates less high order harmonics than using the shaping filter.

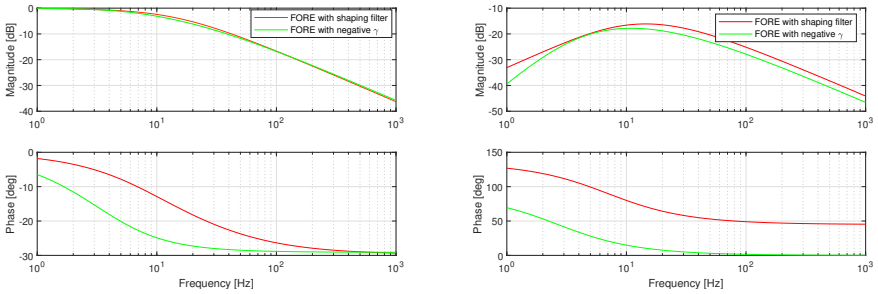

(a) The 1st order DFs (b) The 3rd order DFs

Figure E.2: Comparison of the FORE with the shaping filter and with negative reset value

More investigations about using shaping filters to get less phase lag need to be done in future.

F

System Overview

This appendix provides an overview of the experiment setup and the identification result.

F.1. Setup

The setup is a Four Flexure Cross Hinges(FFCH) system built by Arjan [18], a former graduate student at HTE department. The side view and the top view of the plant are shown in Fig. F.1.

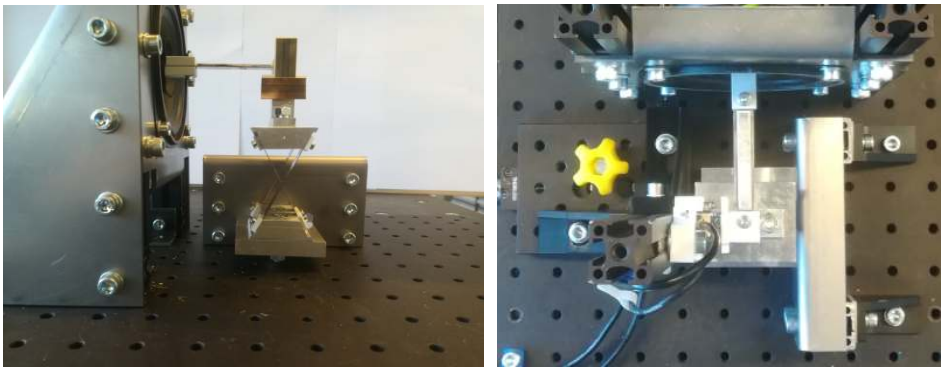

(a) Side view (b) Top view

Figure F.1: The FFCH setup

The base of the hinge is fixed on a vibration isolation table. The top end is connected with a Visaton FR10-4 loudspeaker through a beam and actuated by a Lorenz actuator inside. In this thesis, the actuator is used to control the displacement of FFCH in x direction. The horizontal position is measured by a Mercury M2000 reflective linear encoder. The resolution of this sensor is 100nm. The required controller is compiled using FPGA module through Labview interface and implemented via compact RIO real-time hardware. The

schematic diagram of the complete control system is shown in Fig. F.2.

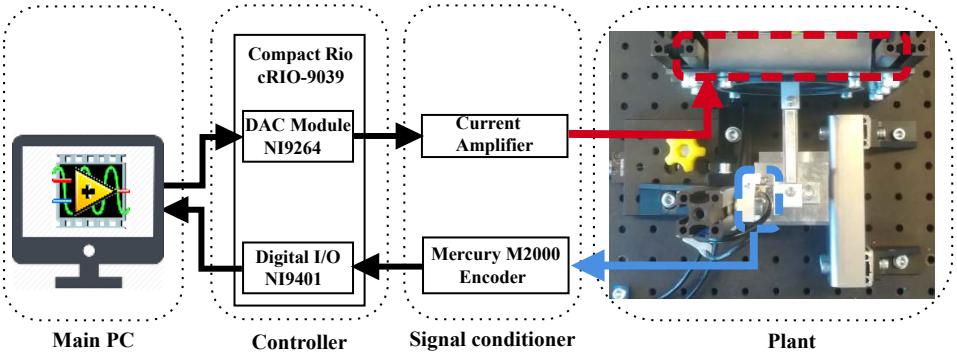

Figure F.2: Schematic overview of the experimental setup

F.2. Identification

To get the frequency response of this system, the system identification is done by exciting the system with a chirp signal. This chirp signal increases from 1Hz to 1000Hz with the increase fraction of 2% per second. The data is logged in every $50\mu s$ and used to obtain transfer function of the system using tfestimate function by MATLAB.

The time domain response of the plant with the input chirp signal is shown in Fig. F.3.

As shown in Fig. F.4, this system is identified as a second order mass-spring-damper system with the estimated transfer function:

$$P(s) = \frac{1}{1.077 \times 10^{-4} s^2 + 0.0049 s + 4.2218} \tag{F.1}$$

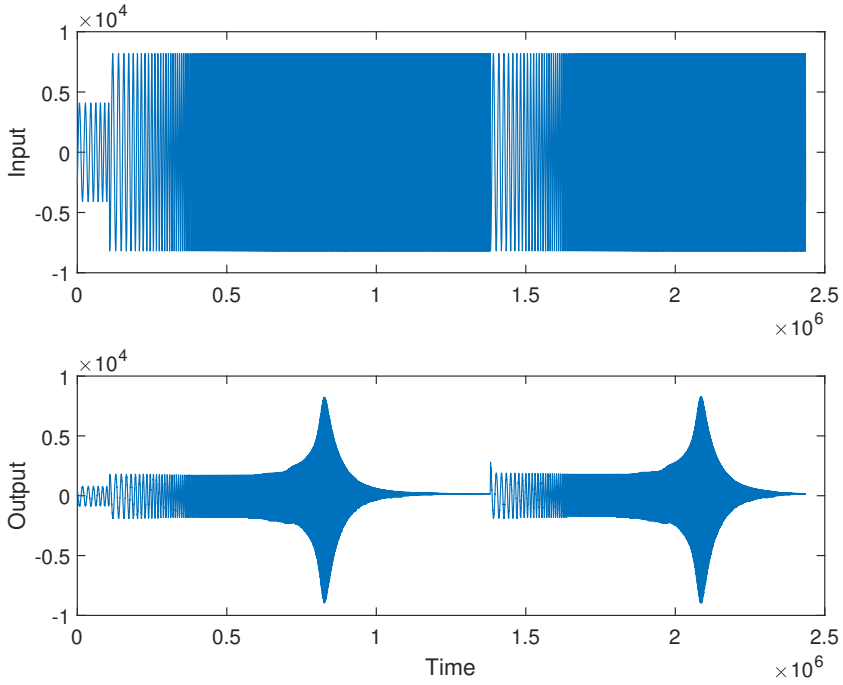

Figure F.3: Time domain response of the experimental setup

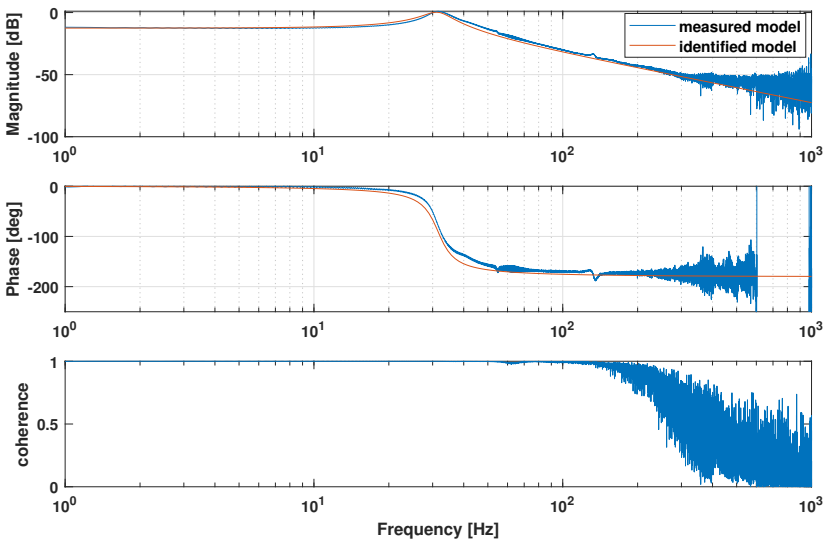

Figure F.4: Frequency domain response of the experimental setup with the estimated transfer function

F

G

Matlab Code and Simulink Model

In this appendix, the MATLAB codes and SIMULINK models used in this thesis are given.

G.1. HOSIDOFs.m

This code is used to calculate HOSIDOFs of a reset element when we have shaping filter in the reset branch.

```
function [G] = HOSIDOFs(sys, Ar, n, phi, freqs)
% Calculate DF for a reset element
% when Input:sin(wt+phi)   and   Reset by sin(wt)
% sys is the reset element described in state space
% A_r is the amount of reset you want to achieve (typical 0)
% phi is the phase shift
% n is the order of the describing function
% freqs is the frequency you want to calculate (rad/s)

% Chengwei Cai - TU Delft - 14.May.2019
 if (mod(n,2) == 0)
        G = 0;
        return;
    end

    A = sys.a; B = sys.b; C = sys.c; D = sys.d;

    G = zeros(1,numel(freqs));

    for i=1:numel(freqs)
        w = freqs(i);

        Lambda = w*w*eye(size(A)) + A^2;
        LambdaInv = inv(Lambda);

        Delta = eye(size(A)) + expm(A*pi/w);
        DeltaR = eye(size(A)) + Ar*expm(A*pi/w);

```

```
29          GammaR = inv(DeltaR)*Ar*Delta*LambdaInv;
30
31          Theta=A*sin(phi)+w*cos(phi)*eye(size(A));
32
33          ThetaD = (-2*w/pi)*Delta*Theta*(GammaR-LambdaInv);
34
35          if (n==1)
36              G(i) = exp(-j*phi)*C*inv(j*w*eye(size(A)) - ...
                    A)*(exp(j*phi)*eye(size(A)) + j*ThetaD)*B;
37
38          else
39              % J1 and J2 dissappear
40              G(i) = exp(-j*phi)*C*inv(j*w*n*eye(size(A)) - A)*j*ThetaD*B;
41          end
42      end
43
44      if (n == 1)
45          G = G + D;
46      end
47  end
```

G.2. Identification.m

This code is used to identify the frequency response of the setup from the data obtained from experiment.

```
1  %identification of the setup
2  % Chengwei Cai - TU Delft - 14.May.2019
3       da=load('data.lvm');
4  u=da(:,1);
5  y=da(:,2);
6
7  [T,f]=tfestimate(u,y,[],[],[],2e4);
8  [C,f]=mscohere(u,y,[],[],[],2e4);
9
10 ax1=subplot(3,1,1);
11 semilogx(f,20*log10(abs(T)));hold on; grid on;
12
13 ylabel ( 'Magnitude [dB]' ) ;
14
15 ax2=subplot(3,1,2);
16 semilogx(f,radtodeg(unwrap(angle(T))));hold on; grid on;
17
18 ylabel ( 'Phase [deg]' ) ;
19
20 ax3=subplot(3,1,3);
21 semilogx(f,C)
22
23 ylabel ('coherence');
24 xlabel('Frequency [Hz]');
25
26 linkaxes ( [ ax1 , ax2 ,ax3] , 'x' )
```

G.3. Sensitivityfunction.m

This code is used to run the real-time simulation of the system and plot the new sensitivity functions for different sequences.

```
%% Closed-loop simulation
%% parameters of the cross flexure
%% Chengwei Cai - TU Delft - 14.May.2019
m=1.077e-4;
c=0.0049;
k=4.2218;

%% calculate Kp
w_c=100*2*pi; %bandwidth
w_d=w_c/4; %corner frequency of Differentiator
w_r=w_d/1.62; %corner frequency of FORE
w_i=w_c/10; %corner frequency of Integrator

A=-w_r; B=w_r; C=1; D=0;
A_rho=0;
sys=ss(A,B,C,D);
s_c=j*w_c;

G_d=(1+s_c/w_d)/(1+s_c/6/w_c);
G_fore=hosidfcalc(sys, A_rho, 1, w_c);
G_i=(s_c+w_i)/s_c;
G_plant=1/(m*s_c^2+c*s_c+k);

G_tot=G_d*G_fore*G_i*G_plant;

k_p=1/abs(G_tot);

%% discretize

Ts=1/20000; %sampling time

% D element
D=tf([1/(w_d),1],[1/6/w_c,1]);
D_z=c2d(D,Ts,'tustin');
[numD, denD] = tfdata (D_z, 'v') ;

% I element
I=tf([1,w_i],[1,0]);
I_z=c2d(I,Ts,'tustin');
[numI, denI] = tfdata (I_z, 'v') ;

% Reset
R=tf([w_r],[1,w_r]);
R_z=c2d(R,Ts,'tustin');
[ A_R , B_R , C_R , D_R] = ssdata (R_z) ;

%shaping filter
a=1.38;
w_f=300*2*pi;
LPF=tf([1],[1/w_f,1]);
ELead=tf([a/w_c,1],[1/a/w_c,1]);
```

```
EC=LPF*ELead;
EC_z=c2d(EC,Ts,'tustin');
[numEC, denEC] = tfdata (EC_z, 'v' ) ;

%% run simulink to get data
freqs=logspace(0,2.2,50); %Hz
for i=1:numel(freqs)
    f=freqs(i);

T=1/f;

sim('crossflexure.slx');

    load('a1');
    load('a2');
    load('a3');
    load('a4');
    load('a5');
    load('a6');
    load('a7');
    load('a8');


a1max(i,:)=max(a1(2,:))/1000;
a2max(i,:)=max(a2(2,:))/1000;
a3max(i,:)=max(a3(2,:))/1000;
a4max(i,:)=max(a4(2,:))/1000;

%control output
a5max(i,:)=max(a5(2,:));
a6max(i,:)=max(a6(2,:));
a7max(i,:)=max(a7(2,:));
a8max(i,:)=max(a8(2,:));

end

%%

figure(3)
semilogx( freqs , 20*log10(a1max),'linewidth',2) ; hold on ; grid on;
semilogx( freqs , 20*log10(a2max),'linewidth',2) ; hold on ; grid on;
semilogx( freqs , 20*log10(a3max),'linewidth',2) ; hold on ; grid on;
semilogx( freqs , 20*log10(a4max),'linewidth',2) ; hold on ; grid on;

legend('Lead-Reset-Lag','Lag-Reset-Lead',...
'Reset-Lead-Lag','Lead-Lag-Reset');
ylabel ( 'error / reference [dB]' ) ;
xlabel ( 'Input frequency [Hz]' ) ;


figure(4)
semilogx( freqs , (a5max),'linewidth',2) ; hold on ; grid on;
semilogx( freqs , (a6max),'linewidth',2) ; hold on ; grid on;
semilogx( freqs , (a7max),'linewidth',2) ; hold on ; grid on;
semilogx( freqs , (a8max),'linewidth',2) ; hold on ; grid on;

legend('Lead-Reset-Lag','Lag-Reset-Lead',...
```

```
109 'Reset-Lead-Lag','Lead-Lag-Reset');
110 ylabel ( 'control output (pulse)' ) ;
111 xlabel ( 'Input frequency [Hz]' ) ;
112 title('control output')
```

G.4. hosidfcalc.m

This code is provided by Kars Heinen. It is used to calculate HOSIDOFs of a reset element without shaping filter.

```
1   function [G] = hosidfcalc(sys, Ar, n, freqs)
2   % G = hosidfcalc(SYS, AR, N, FREQS, CLOL)
3   % Calculated the higher order (n) describing function for a reset ...
        system.
4   %
5   % SYS is the reset element described in state space
6   % AR is the amount of reset you want to achieve (typical 0)
7   % N is the describing function order
8   % FREQS contains the frequencies the describing function is ...
        calculated for
9
10  % Kars Heinen - TU Delft - 2018
11
12  % to do; replace inv() by 'matlab \' for faster results
13
14  % odd orders will be skipped
15  if (mod(n,2) == 0)
16      G = 0;
17      return;
18  end
19
20  A = sys.a; B = sys.b; C = sys.c; D = sys.d;
21
22  G = zeros(1,numel(freqs));
23
24  for i=1:numel(freqs)
25      w = freqs(i);
26
27      Lambda = w*w*eye(size(A)) + A^2;
28      LambdaInv = inv(Lambda);
29
30      Delta = eye(size(A)) + expm(A*pi/w);
31      DeltaR = eye(size(A)) + Ar*expm(A*pi/w);
32
33      GammaR = inv(DeltaR)*Ar*Delta*LambdaInv;
34
35      ThetaD = (-2*w*w/pi)*Delta*(GammaR-LambdaInv);
36
37      if (n==1)
38          G(i) = C*inv(j*w*eye(size(A)) - A)*(eye(size(A)) + ...
                j*ThetaD)*B;
39      else
40          % J1 and J2 dissappear
41          G(i) = C*inv(j*w*n*eye(size(A)) - A)*j*ThetaD*B;
```

```
42              end
43          end
44
45          if (n == 1)
46              G = G + D;
47          end
48      end
```

G.5. Simulink model

This model is used to simulate the closed-loop performance of the system under different level of noise.

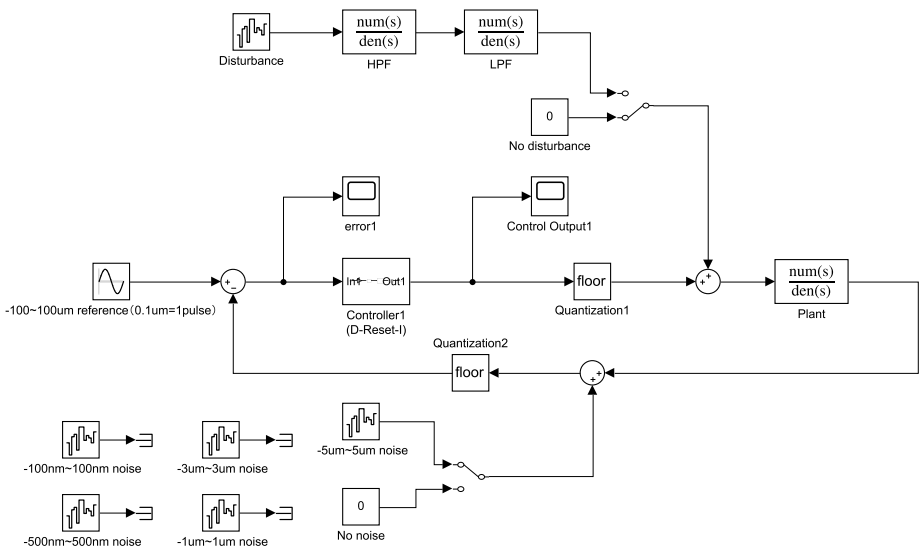

Figure G.1: crossflexure.slx

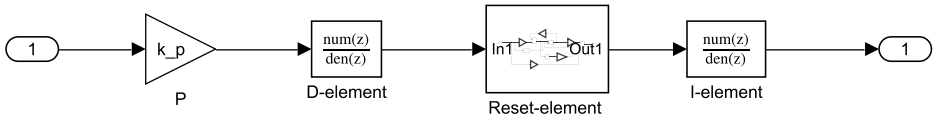

Figure G.2: Controller1(D-Reset-I).slx

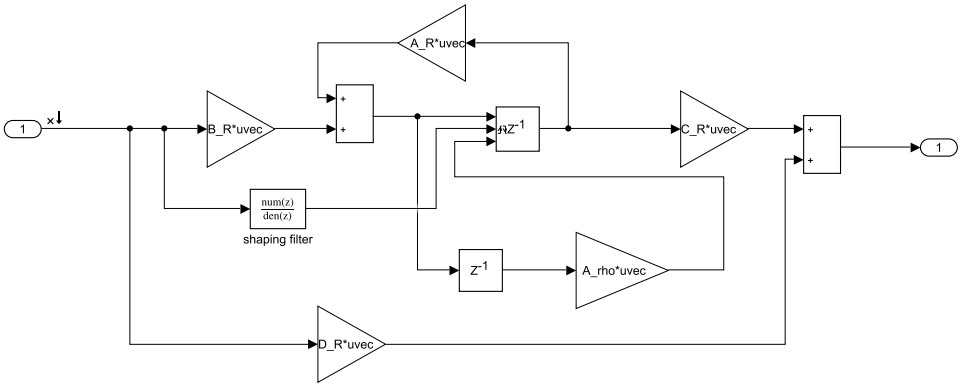

Figure G.3: Reset-element.slx

Bibliography

[1] R. M. Schmidt, G. Schitter, and A. Rankers, *The Design of High Performance Mechatronics-: High-Tech Functionality by Multidisciplinary System Integration*. Ios Press, 2014.

[2] G. E. Moore *et al.*, "Cramming more components onto integrated circuits," 1965.

[3] ASML, "Our role in the semiconductor industry." https://www.asml.com/our-role-in-the-semiconductor-industry/en/s45818?dfp_fragment=stratman_1, 2012. [web].

[4] K. J. Åström and T. Hägglund, "The future of PID control," *Control engineering practice*, vol. 9, no. 11, pp. 1163–1175, 2001.

[5] S. Skogestad and I. Postlethwaite, *Multivariable feedback control: analysis and design*, vol. 2. Wiley New York, 2007.

[6] L. Chen, N. Saikumar, S. Baldi, and S. H. HosseinNia, "Beyond the waterbed effect: Development of fractional order crone control with non-linear reset," in *2018 Annual American Control Conference (ACC)*, pp. 545–552, IEEE, 2018.

[7] M. Zarghami and S. HassanHosseinNia, "Fractional order set point regulator using reset control: Application to egr systems," in *Proceedings of the 2017 The 5th International Conference on Control, Mechatronics and Automation*, pp. 35–41, ACM, 2017.

[8] S. H. HosseinNia, I. Tejado, and B. M. Vinagre, "Basic properties and stability of fractional-order reset control systems," in *2013 European Control Conference (ECC)*, pp. 1687–1692, IEEE, 2013.

[9] S. H. HosseinNia, I. Tejado, and B. M. Vinagre, "Fractional-order reset control: Application to a servomotor," *Mechatronics*, vol. 23, no. 7, pp. 781–788, 2013.

[10] L. Marinangeli, F. Alijani, and S. H. HosseinNia, "Fractional-order positive position feedback compensator for active vibration control of a smart composite plate," *Journal of Sound and Vibration*, vol. 412, pp. 1–16, 2018.

[11] J. Clegg, "A nonlinear integrator for servomechanisms," *Transactions of the American Institute of Electrical Engineers, Part II: Applications and Industry*, vol. 77, no. 1, pp. 41–42, 1958.

[12] Y. Guo, Y. Wang, and L. Xie, "Frequency-domain properties of reset systems with application in hard-disk-drive systems," *IEEE Transactions on Control Systems Technology*, vol. 17, no. 6, pp. 1446–1453, 2009.

[13] L. Hazeleger, M. Heertjes, and H. Nijmeijer, "Second-order reset elements for stage control design," in *2016 American Control Conference (ACC)*, pp. 2643–2648, IEEE, 2016.

[14] I. Horowitz and P. Rosenbaum, "Non-linear design for cost of feedback reduction in systems with large parameter uncertainty," *International Journal of Control*, vol. 21, no. 6, pp. 977–1001, 1975.

[15] P. Nuij, O. Bosgra, and M. Steinbuch, "Higher-order sinusoidal input describing functions for the analysis of non-linear systems with harmonic responses," *Mechanical Systems and Signal Processing*, vol. 20, no. 8, pp. 1883–1904, 2006.

[16] K. Heinen, "Frequency analysis of reset systems containing a clegg integrator: An introduction to higher order sinusoidal input describing functions," 2018.

[17] P. Lambrechts, M. Boerlage, and M. Steinbuch, "Trajectory planning and feedforward design for electromechanical motion systems," *Control Engineering Practice*, vol. 13, no. 2, pp. 145–157, 2005.

[18] A.van.Unen, "Dynamic responses of centimetre scale parallel-and-cross flexures." http://aiweb.techfak.uni-bielefeld.de/content/bworld-robot-control-software/, 2019. [Online].